Roles of microRNA-15 family in normal and pathological late lung development

Inauguraldissertation

zur Erlangung des Grades eines Doktors der Humanbiologie

des Fachbereichs Medizin

der Justus-Liebig-Universität Gießen

vorgelegt von

Elpidoforos Sakkas

aus Thessaloniki, Griechenland

Gießen, 2016

Roles of microRNA-15 family in normal and pathological late lung development

Aus dem

Max-Planck-Institut für Herz- und Lungenforschung, Bad Nauheim

Leiter/Direktor: Prof. Dr. W. Seeger

Betreuer: Prof. Dr. Seeger
Gutachter: Prof. Dr. Müller
Prüfungsvorsitz: Prof. Dr. Dr. Stieger
Prüfungsmitglied: Prof. Dr. Neubauer

Tag der Disputation: 03.02.2016

I. Table of contents

II. List of figures

III. List of tables

IV. List of abbreviations

AT II	alveolar epithelial type II
AGO	argonaute
APS	ammonium persulfate
ALK	activin receptor-like kinase
bp	base pair(s)
BPD	bronchopulmonary dysplasia
BMP	bone morphogenic protein
BSA	bovine serum albumin
COPD	chronic obstructive pulmonary disease
DGCR8	DiGeorge critical region 8
DMEM	Dulbecco's modified Eagle's medium
DTT	dithiothreitol
ECM	extracellular matrix
EDTA	ethylene dinitril *o*-N,N,*N*′,*N*′-tetraacetic acid
FGF	fibroblast growth factor
g	gram(s)
h	hour(s)
IPF	interstitial pulmonary fibrosis
JNK	c-Jun N-terminal kinase
kg	kilogram(s)
LNA	locked nucleic acid
MAD	mothers against decapentaplegic
MAPK	mitogen-activated protein kinase
mg	milligram(s)
MH	MAD homolog
min	minute(s)
ml	milliliter(s)
mM	millimolar
mV	millivolt(s)
ng	nanogram(s)
nM	nanomolar
nm	nanometer(s)
nt	nucleotide
P	post-natal day

PBS	Phosphate-buffered saline
qPCR	quantitative PCR
PCR	polymerase chain reaction
Pol II	RNA polymerase II
Pre-miR	precursor microRNA
Pri-miR	primary microRNA
PMA	post-menstrual age
rpm	revolutions per minute
qPCR	quantitative PCR
RDS	respiratory distress syndrome
RISC	RNA induced silencing complex
RNAi	RNA interference
rpm	revolutions per minute
R-SMAD	receptor SMAD
RT	room temperature
s	second(s)
SDS	sodium dodecyl sulfate
SEM	standard error of the mean
SPARC	protein acidic rich in cysteine
SMA	smooth muscle actin
SMURF	SMAD ubiquitin related factor
SUR	uniform random sampling
TGFRI	TGF-β receptor type I
TGFRII	TGF-β receptor type II
TEMED	N,N,*N´*,*N´*-tetramethylethane-1,2-diamine
TGF-β	transforming growth factor-β
UTR	untraslated region
VLBW	very low birth weight
XPO5	Exportin-5
µg	microgram(s)
µl	microliter(s)
µM	micromolar
µm	micrometer

1 Introduction

1.1 Lung development

The lungs are the organs necessary for breathing, although initially appear to be unnecessary for intrauterine existence. Nevertheless, the lungs are programmed to function immediately after birth. During fetal development, the branching and growth of the lungs are under the direction of the mesenchyme. This characteristic is also found in kidney, where epithelial-mesenchymal interaction is important for the normal development of the lungs (Koshida and Hirai 1997).

Lung development is a lengthy process passing through different stages until reaches maturation. Development starts in the third week of the embryonic stage and it is approximately completed at 2-3 years of age where alveoli and total lung structure are fully matured. Over the past years, there is strong evidence that the alveoli number and lung surface area continue increasing until adulthood (Hislop 2002).

1.2 Phases of lung development

In humans, the respiratory tract passages are divided into 23 division points or generations (Fig 1-1). At every generation, one airway is divided into two smaller airways. The human respiratory tree consists on average of 23 generations, while the respiratory tree of the mouse has up to 13 generations. The last generations include the respiratory bronchioles, alveolar ducts and alveoli which are specialized structures for proper gas exchange (Kitaoka et al. 1996). Based on histological characteristics, there are five developmental stages that have been defined: the embryonic, the pseudoglandular, the canalicular, the saccular and the alveolar stage. The early stages are characterized by branching morphogenesis, while the later stages are characterized by vascularization and the formation of thin air-blood interfaces responsible for gas exchange (Boucher et al. 2009). During the pseudoglandular stage, the epithelial tube undergoes branching, generating the respiratory part to the level of distal bronchioles. During the canalicular stage, the distal airway bronchioles are formed with a significant proximal to epithelial differentiation. This is the stage where mesenchymal cells begin to develop into fibroblasts, lipofibroblasts and myofibroblasts (Goldin and Wessells 1979).

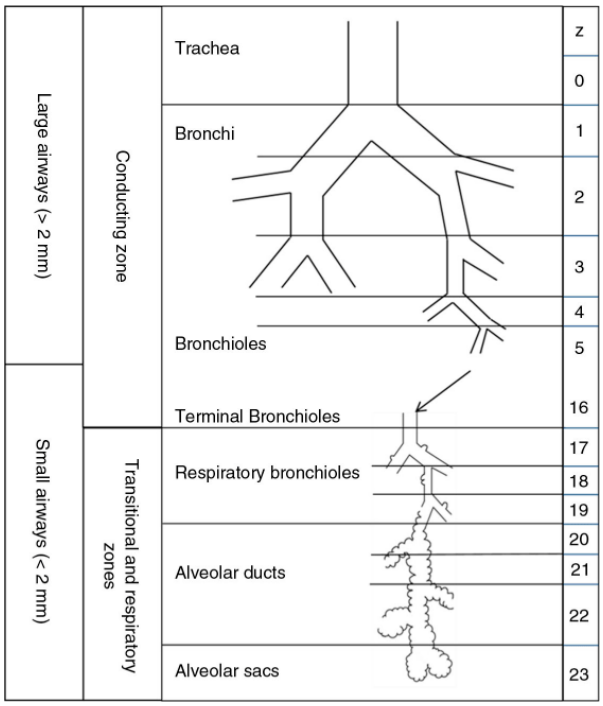

Figure 1-1 Lung development and respiratory tract generations.
According to their function, the respiratory tract passages are divided into conducting and respiratory zones. Conducting zones consist of 16 generations including bronchi, bronchioles and terminal bronchioles. The respiratory zone consists of seven generations including respiratory bronchioles, alveolar ducts and alveolar sacculi (Weibel 1963).

By the end of canalicular stage (Fig 1-2), between weeks 16 and 25, respiration is possible, although the survival rates of newborns delivered at this stage are low. Between week 25 and birth, during the saccular stage, there is a massive expansion of airspaces and pneumocytes start producing surfactant. At this stage, newborns have a much higher probability of survival. However, even at this stage, respiratory support for the newborns is necessary. The positive pressure ventilation with a high oxygen gas can lead to chronic lung injury and is a major factor for the development of bronchopulmonary dysplasia (BPD) (Coalson 2006).

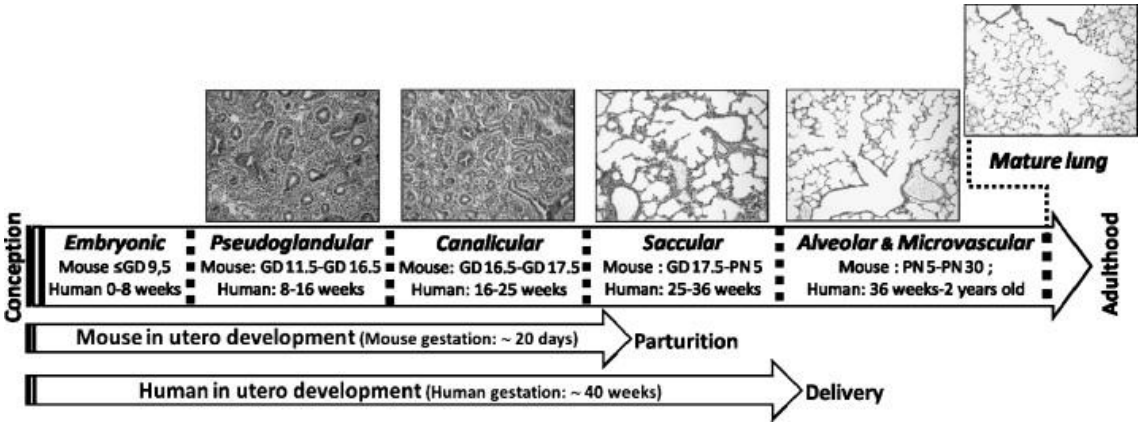

Figure 1-2 Overview of the stages in normal lung development.
There is a significant expansion of the lung in the saccular stage, and a generation of an increasing number of alveoli of a smaller size, between the saccular phase and the mature lung (Boucher et al. 2009).

During the final stage of lung development, the process of septation takes place. This is the process by which new alveolar sacs are generated, and can be seen in detail in Figure 1-3, where the wall of an existing alveolus gives rise to a new septum, which then extends and grows to form the wall of a new alveolus. The alveolarization stage leads to a honeycomb appearance accompanied by a significant increase in gas exchange surface area. After septation has been completed, the final phase of late lung development is the consolidation of the capillary layers, in the stage of "microvascular maturation" (Fig 1-3 D). In humans the alveolar stage starts during the fetal period but in rodents alveolarization is predominantly a post-natal (P) event.

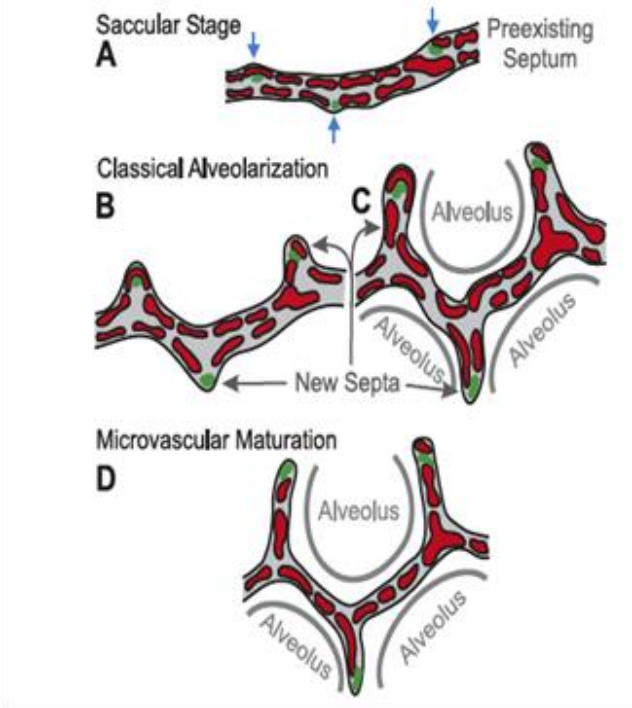

Figure 1-3 Structural mechanism for late lung alveolarization.
The points of formation of new "secondary septa" are indicated by a blue arrow. Panels (B) and (C) illustrate how the newly formed secondary septa lead to the formation of a new alveolus (Schittny et al. 2008).

1.3 MicroRNAs and lung development

MicroRNAs belong to a large group of non-coding small RNAs and are 20-22 nucleotides (nt) in length. MicroRNAs were first described in 1993 as negative regulators in *Caenorhabditis elegans*, with Lin-14 being the first described microRNA gene, influencing the timing of the larva to adult switch. Since then, thousands of microRNAs have been identified that are highly conserved across species and have been established as major regulators of gene expression. Studies up to this point have demonstrated that one third of human genes are regulated by microRNAs. These genes are mainly involved in developmental timing, cellular differentiation, immune regulation, cell cycle and apoptosis (Fineberg et al. 2009, Gangaraju and Lin 2009, Lewis et al. , Mattes et al. 2008).

1.3.1 Biogenesis and function of microRNAs

In the nucleus, a primary microRNA (pri-miR) is transcribed from microRNA genes and is synthesized by RNA polymerase II (Cai et al. 2004, Vicencio et al. 2004). Expression of different microRNAs is under the control of transcription factors, for example c-Myc or p53 (He et al. 2007, O'Donnell et al. 2005), or depends on the methylation of microRNA promoters (Lujambio et al. 2008, Saito et al. 2006). Additionally, it has been shown that each microRNA located in the same genomic cluster can be transcribed and regulated independently (Song and Wang 2008). The primary microRNA is processed by the RNase III enzyme Drosha and the DGCR8 (DiGeorge critical region 8) protein, leading to a smaller sequence (~ 70 nt) defined as a precursor microRNA (pre-miR).

After the completion of the process in the nucleus, the pre-miR is transferred into the cytoplasm by Exportin-5 (XPO5) in complex with Ran-GTP (Yi et al. 2003). Knockdown of Exportin-5 leads to lower abundance of mature microRNA sequences, indicating that Exportin-5 protects pre-miRs against nuclear digestion (Lund et al. 2004, Yi et al. 2003).

In the cytoplasm, the pre-miR is cleaved by another RNase III enzyme (Dicer) and generates roughly a 22-nt double stranded miR duplex molecule. Deletion of Dicer decreases the production of mature miRs (Grishok et al. 2001, Hutvagner et al. 2001). This miR duplex is then separated into two single strands, the mature strand (miR) and the passenger strand (miR*). The mature microRNA is incorporated into the RNA induced silencing complex (RISC) as a template for the target mRNA and the passenger microRNA is degraded (Fig 1-4). The RNA induced silencing complex is a large protein complex and includes the argonaute protein (AGO), the transactivating response RNA binding protein (TRBR) and the fragile X mental retardation protein (FMRP1). The Argonaute 2 is an isoform of the AGO protein and it is the one responsible for the cleavage of the target mRNA. The mature sequence of the microRNAs binds to the 3 prime untranslated region (UTR) of the target mRNA and inhibits the gene expression by two different mechanisms; either by mRNA degradation or by translational repression. RISC inhibits translation by recruiting factor eIF6, causing detachment of the 80S ribosomal complex (Iwasaki et al. 2009). Deadenylation of mRNA is another mechanism triggered by AGO protein isoforms and leads to degradation of the target mRNA.

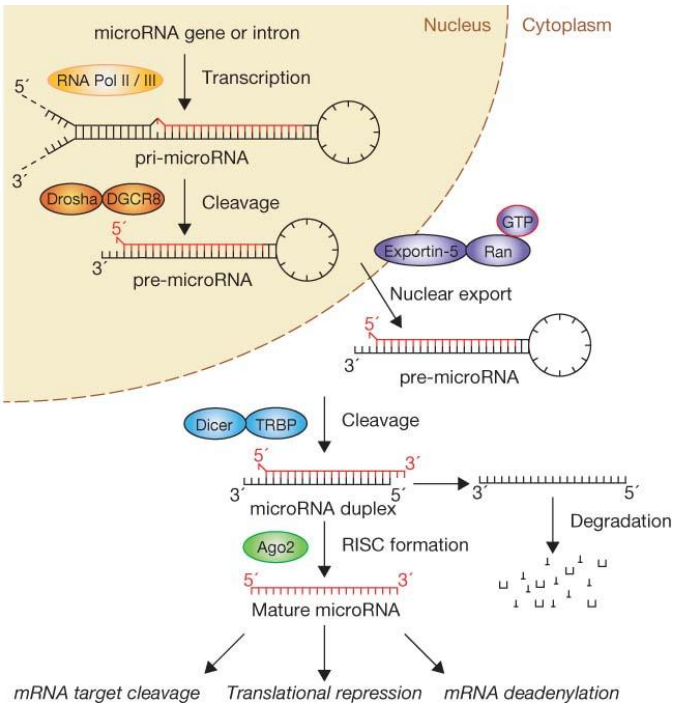

Figure 1-4 The canonical pathway of microRNA processing has been associated with all mammalian microRNAs.

This pathway includes the generation of a pri-miR by RNA polymerase II and the cleavage of the pri-miR by the Drosha-DGCR8 complex in the nucleus. The resulting sequence (pre-miR) is exported to the cytoplasm by Exportin-5. In the cytoplasm, the enzyme Dicer cleaves the pre-miR sequence to a mature form. The mature sequence of the microRNA is loaded with Argonaute proteins, and the complex targets mRNAs through cleavage, translational repression or deadenylation. The passenger strand is degraded and it is not functional (Winter et al. 2009). GTP, guanine triphosphate; Ran, RA-related nuclear protein.

1.3.2 MicroRNAs in the lung

There is an array of studies that have profiled the expression of several microRNAs at various stages of lung development. One of the first studies that demonstrated the implication of microRNAs in lung development was conducted by Harris et al. (Harris et al. 2006). A conditional knock-out mouse ablated Dicer after the initiation of lung branching. The mutant lines demonstrated an extensive arrest in branching with an abnormal growth of the epithelial tube. Recently, Dong et al. performed a systematic clustering and expression profiling of microRNAs, target

mRNAs and proteins at different stages of lung development (Dong et al. 2012). According to the study, most of the microRNAs that increased their expression levels, correlated with a down-regulation of their predicted target mRNAs. In other cases, over half of the proteins that were analyzed, a down regulation occurred independently of changes in mRNA levels. These findings support the hypothesis that the inhibition of translation is an important mechanism of microRNAs (Dong et al. 2010). There are not many studies addressing the function of microRNAs in later stages of development. Most of the studies focus on embryonic development; for example Carraro et al. have proposed a role for the miR-17~92 cluster during early lung development, through regulation of the fibroblast growth factor (FGF) and the effects on E-cadherin expression (Carraro et al. 2009). In that study it was demonstrated that a down- regulation of miR-17, miR-20a and miR-106b disrupts embryonic lung branching through E-cadherin redistribution. The E-cadherin expression and distribution are important for epithelial cell organization during lung branching. It has also been demonstrated that miR-17 negatively regulates FGF10 signaling by targeting Mapk14 and Stat3 (Liu Yuru et al. 2008).

For late lung development, and specifically for the alveolar stage, there are only two studies that have investigated the expression levels of microRNAs. Williams et al. analyzed the differential expression of microRNAs between post-natal (P) day 1 and P14 in mice and humans (Williams et al. 2007). Microarray profiling of mouse lungs revealed an up-regulation of 14 microRNAs in neonatal lungs and an up-regulation of 30 microRNAs in adult tissues. Few of the most highly regulated microRNAs were miR-335, miR-154, miR-370 and miR-337. MicroRNA expression levels were similar in mouse and human lungs, suggesting that microRNA expression is evolutionary conserved among species during late lung development (Williams et al. 2007). In the second study, Bhaskaran et al. demonstrated that miR-127 was the highest expressed microRNA just before and after birth, during the alveolar stage in rats. It was observed that miR-127 expression has a tendency to shift from mesenchymal to epithelial cells in the developing lung. That suggests a role for this microRNA in cellular processes such as cell differentiation (Bhaskaran et al. 2009).

1.4 Bronchopulmonary dysplasia

Bronchopulmonary dysplasia is also referred as neonatal chronic lung disease and is characterized as a chronic pulmonary disorder of prematurely born infants with a very low birth weight. Bronchopulmonary dysplasia was first described in 1967 by W.H. Northway and colleagues as a severe complication of preterm birth (Northway et al. 1967), and since then it has been noted as a major cause of morbidity in neonatal intensive care units. The disease has a varied degree of severity including recurrent pulmonary infections, impaired neurological development and pulmonary hypertension. There are two types of BPD that have been described, the 'classic' or 'old' has been substituted by the milder 'new' BPD. The improved perinatal care has led to this transformation that also reduced the morbidity rates. The 'old' BPD was characterized by extensive inflammatory changes and the 'new' by a decreased degree of secondary alveolar septation and an arrest of late lung development. According to Northway, there are 4 stages of BPD, mainly defined by clinical characteristics. Stage I (usually 2-3 days) noted as respiratory distress syndrome (RDS); stage II (4-10 days) noted as regeneration; stage III (11-20 days) noted as transition to chronic disease and stage IV (more than one month) noted as a chronic lung disease. Later, Bancalari et al. attempted to define BPD as a disorder among infants who received supplemental oxygen at 28 days postnatal (Bancalari and Claure 2006). In 2000, the National Institute of Child Health and Human Development (NICHD) redefined BPD (Fig 1-5): BPD was for the first time characterized by the severity of the disease. The disease was defined and categorized into mild, moderate and severe BPD (Table 1-1).

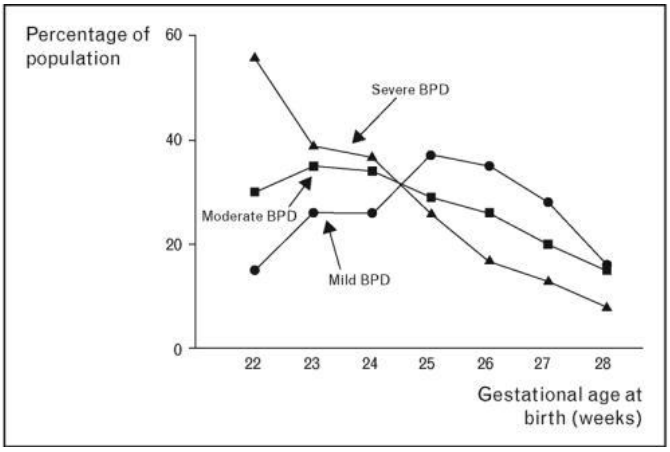

Figure 1-5: Severity of BPD, based on the National Institutes of Health 2000 conference definition.

9575 infants were categorized according to severity of BPD; sixty eight percent of these infants had BPD. Severity of BPD decreased as gestational age increased (Jobe 2011).

In 2004, Walsh et al. developed a physiological test that established the need for supplemental oxygenation (Walsh et al. 2004). According to the algorithm for the physiological test, infants receiving inspired oxygen concentration with a fraction of >0.3 are categorized as having BPD, and infants with a fraction of <0.3 must undergo an oxygen challenge test to determine if they develop BPD. Bronchopulmonary dysplasia is a disease with a multifactorial causality, and the factors include prematurity, gender, genetic predisposition, mechanical ventilation and postnatal infection.

Table 1-1 Diagnostic criteria and categorization of the severity of BPD (Jobe 2011). wk, week; PMA, postmenstrual age.

<32 wk Gestational age	>32 wk Gestational age	Diagnosis
Breathing room air at 36 wk PMA or discharge, whichever comes first	Breathing room air by 56 days postnatal age or discharge, whichever comes first	Mild
Need for <30% O_2 at 36 wk PMA or discharge, whichever comes first	Need for <30% O_2 at 56 days postnatal age or discharge, whichever comes first	Moderate
Need for >30% O_2, positive pressure, or both at 35 wk PMA or discharge, whichever comes first	Need for >30% O_2, positive pressure, or both at 56 days postnatal age or discharge, whichever comes first	Severe

1.4.1 Epidemiology

The improved perinatal care reduced the respiratory clinical incidents and the characterization of BPD has changed throughout the years. The diagnostic markers of the disease are subjects in multiple studies making it possible for the future to prevent and possibly treat the disease.

A study in 2001 noted that 23% of newborns with a birth weight below 1500 g are oxygen dependent at 36 weeks (Lemons et al. 2001). In 2003, another study noted that 53% of infants born before 28 weeks of gestational age were oxygen-dependent at 36 weeks (Schreiber et al. 2003).

As a long-term outcome, children with BPD have higher rates of educational and behavioral impairments and also reduced lung function throughout childhood. Short et al. supported that BPD has long term effects on cognitive and academic achievement. Infants with a very low birth weight (VLBW) have motor skill impairment and linguistic developmental delay compared to healthy controls (Short et al. 2003). Respiratory symptoms in patients with BPD persist until adulthood and these subjects have a higher chance of developing chronic obstructive pulmonary disease (COPD) (Short et al. 2003).

1.5 TGF-β signaling pathway

Transforming growth factor β is a key growth factor conserved amongst vertebrates, regulating embryonic development and organogenesis, wound repair, cell proliferation, apoptosis and cell differentiation. TGF-β is secreted in an inactive form and deposited into the extracellular matrix (ECM) where is coupled to latent TGF-β binding proteins. The activated form of TGF-β can be recognized by TGF-β receptors 1 (TGFRI) and 2 (TGFRII). Transforming growth factor receptor 1 includes activin receptor like kinase ALK1 and ALK5, TGF-β receptor 2 belongs to the TGFRII family and betaglycan and endoglin represent type III receptors. Upon ligand binding, receptor I and II undergo heterodimerization in a series of activation events. Specifically, the ligand is recognized by the TGF-β receptor 2 and initiates the phosphorylation of TGF-β receptor 1, resulting in the association of both molecules. Subsequently, receptor 1 phosphorylates the SMAD2 protein (homologs of the

Drosophila protein mothers against decapentaplegic) which is docked to the receptor complex (Fig 1-6). During the canonical TGF-β signaling, activated SMAD2 and SMAD3 proteins form a complex with SMAD4 and translocate into the nucleus and act as transcription factors. The SMAD2 and SMAD3, which are also referred as receptor SMADs (R-SMADs), share similar structures with the presence of MH1 and MH2 domains on the N and C-terminus respectively. The MH1 region is responsible for DNA binding while the MH2 region regulates protein-protein interactions. The TGF-β superfamily is not limited only to SMAD pathway but it can also mediate signaling through non-SMAD pathways, specifically through mitogen activated protein kinase (MAPK) pathways, including p38 and Jun N-terminal kinase (JNK) (Miyazono et al. 2005). Once the pathway is activated, there is a negative feedback mechanism caused by another group of SMAD proteins and can regulate the signaling. The proteins responsible for this inhibitory feedback are named inhibitory SMADs (I-SMADs) and consist of SMAD6 and SMAD7. The I-SMADs lack the MH1 domain and are both stimulated by TGF-β and BMP ligands; I-SMADs compete with R-SMADs following an association with the respective type I receptors and negatively regulate TGF-β family signals (Imamura et al. 1997, Nakao et al. 1997). As a matter of fact, the inhibitory SMADs recruit the E3 ubiquitin ligases, SMAD ubiquitin-related factor-1 (SMURF1) and SMAD ubiquitin-related factor-2 (SMURF2), which are able to ubiquitinate the SMADs and the TGFRI, leading to protein degradation and consequently to inhibition of the signaling. The TGF-β superfamily also stimulates the production of secreted protein acidic rich in cysteine (SPARC), which enhances TGF-β signaling; it also stimulates the production of cystatin C that inhibits TGF-β signaling (Sokol and Schiemann 2004, Sokol et al. 2005).

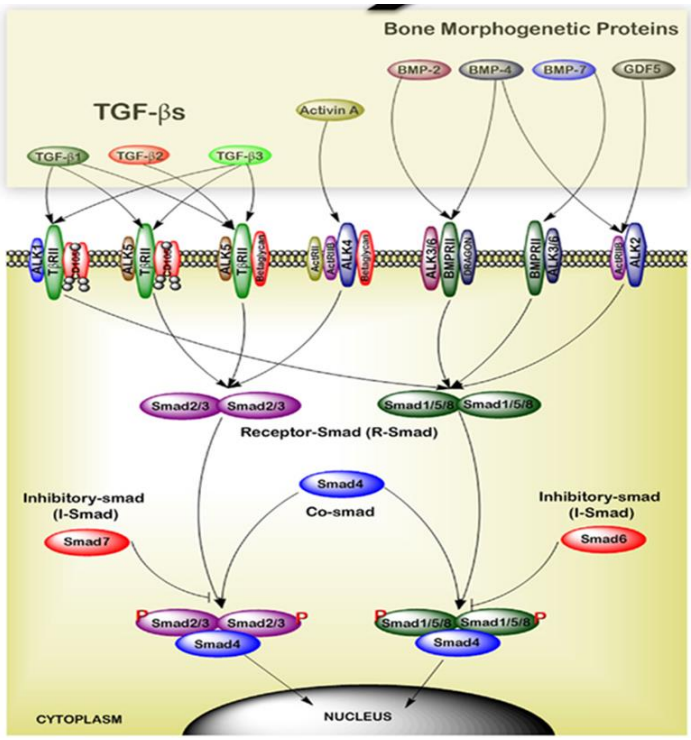

Figure 1-6 Representation of the TGF-β signaling pathway.
Extracellular TGF-β family ligands bind directly to the type II receptor which form heterodimers with the type I receptor. This reaction activates the receptor serine/threonine kinase activity to phosphorylate Smad2/3 complex. The phosphorylation of the receptor activated the Smad2/3 complex leads to formation of heterodimers with partner proteins such as Smad4. Finally, the entire complex translocates to nucleus where activates or inhibits the transcription of target genes (Massague 2012). TGF-β, transforming growth factor; BMP, bone morphogenic protein; Smad, homologs of the *Drosophila* protein mothers against decapentaplegic;

Concerning the inhibitory proteins, which form a part of the current study, it has been reported over the last decade that a balanced expression of SMAD7 levels is necessary for homeostasis during embryonic development and for proper function of many organs (Zhu et al. 2011). For example, deregulation of SMAD7 can cause major developmental defects in cardiovascular morphogenesis and lung branching (Zhu et al. 2011). In terms of potential therapy against fibrosis and the excessive production of ECM components caused by TGF-β, an overexpression of SMAD7 might lead to a promising therapy (Briones-Orta et al. 2011). In a recent study, SMAD7 has been characterized as a microRNA target; activation of TGF-β signaling pathway promotes the expression of the miR-21 in vascular smooth muscle cells and in lung fibroblasts

(Davis et al. 2008, Liu G. et al. 2010). An up-regulation of miR-21 expression decreased SMAD7 expression levels, where antagomirs against miR-21 increased SMAD7 expression in the lung fibroblasts. This finding suggests an involvement of a microRNA in the TGF-β signaling pathway (Liu G. et al. 2010).

1.5.1 Hyperoxia and TGF-β signaling

It has been reported that injury to the developing lung caused by hyperoxia can disrupt major pathways, such as TGF-β signaling, leading to developmental arrest (Alejandre-Alcazar et al. 2007, Kotecha et al. 1995, Lecart et al. 2000). Higher levels of TGF-β ligands have been observed in neonates with BPD undergoing oxygen therapy and in animal models with lung injury (Buckley and Warburton 2002). Also, exposure of alveolar type II (ATII) cells to 95% O_2 promoted the association of Smad2/3/4 complexes with DNA (Nabeyrat et al. 2001), indicating that hyperoxia up-regulates TGF-β signaling. Other studies have reported that up-regulation of TGF-β in rodents result in pulmonary changes that are similar to those observed in BPD (Gauldie et al. 2003, Vicencio et al. 2004). In 2007, Nakanishi et al. reported that TGF-β neutralizing antibodies attenuated the increase in nuclear phosphorylation of SMAD2, a major indicator of TGF-β signaling activation. The neutralization of the overexpression of TGF-β signaling improved alveolarization, ECM assembly and vascular development in the injured lung (Nakanishi et al. 2007). At a cellular level, hyperoxia can induce metabolic changes and can play a key role in the transdifferentiation of lung fibroblasts to myofibroblasts. This transdifferentiation can occur spontaneously but it is noted that is accelerated by exposure to high oxygen concentration (Boros et al. 2002). Specifically, the immature lung lipofibroblasts when exposed to hyperoxia differentiate to a phenotype with contractile elements and a high proliferating potential, referred as myofibroblasts. Myofibroblasts belong to the family of fibroblasts, and highly express α-smooth muscle actin (α-SMA) among other contractile elements, and have been identified as key mediators of idiopathic pulmonary fibrosis (IPF) and other profibrotic conditions (Fallowfield 2011, Hardie et al. 2009, Makinde et al. 2007). The fibroblast phenotype with such properties is TGF-β dependent and arises after chronic epithelial injury or inflammation, two major characteristics of BPD. Bozyk et al, reported that in BPD, alveolar septa are thickened

with collagen and α-SMA produced by myofibroblasts. Periostin is another molecule expressed by myofibroblasts and was co-localized with α-SMA in infants dying from BPD (Bozyk et al. 2012). However, another study reported that a profound deficiency in alveolar myofibroblasts and elastic fibers resulted in the absence of secondary septa and definitive alveoli. That was mainly due to the fact that myofibroblasts failed to migrate from the proximal sites to the peripheral sites of the lung where elastin deposition occurs (Bourbon et al. 2005). To date, there is no study referring to the balance of the number of "accumulated" myofibroblasts in healthy conditions or in disease. Thus, myofibroblasts are essential, as a unique source of connective tissue material during secondary septation but are also involved in fibrotic processes in the reparative mechanisms in response to lung injury.

1.5.2 The role of TGF- β in lung development and BPD

The TGF-β signaling pathway appears to be responsible for a large part of the regulatory balance in lung development (Alejandre-Alcazar et al. 2008). All isoforms of TGF-β, TGF-β1, TGF-β2 and TGF-β3 are expressed early in pulmonary development along with the members of SMAD protein family (Schmid et al. 1991). It has been shown that down regulation of TGF-β receptor 2 and SMAD2/3/4 is associated with increased branching morphogenesis in mouse lung explants (Zhao et al. 1998). However, overexpression of TGF-β1 in the distal pulmonary epithelium led to an arrest in development (Wu et al. 2007). These findings indicate the negative influence that TGF-β1 has on lung branching and that the balance of the TGF-β signaling is important for homeostasis (Zhou et al. 1996). In alveolar epithelial cells, TGF-β1 inhibits proliferation, induces epithelial-to-mesenchymal transition (EMT) and apoptosis (Kasai et al. 2005)**.** During late lung development, chronic exposure to hyperoxia severely decreases alveolarization and vasculogenesis (Nakanishi et al. 2007). This finding is supported by the evidence that the level of TGF-β1 observed in tracheal effluents of premature newborns appears to be elevated in the ones that develop BPD (Kotecha and Kotecha 2012). Neptune et al showed that mice deficient in fibrillin-1 have increased TGF-β signaling and reduced alveolarization (Neptune et al. 2003). Additionally, data suggest that injury of the lung during the saccular stage causes the formation of dysmorphic blood vessels; the expression levels of PECAM-

1, a protein abundant in endothelial cells, has been observed to be abnormally distributed in the septal walls of infants that have died from BPD (Bhatt et al. 2001). It has been reported that TGF-β decreases PECAM-1 expression in the lungs of developing mice (Zeng et al. 2001). Additional studies on the long-term effect of TGF-β signaling and the possible inhibition will further develop approaches in the modulation of pulmonary injury.

2 Hypothesis and aims of the study

In the lung, tissue-specific deletion of Dicer, the enzyme responsible for producing active microRNAs, results in branching arrest and revealed the importance of microRNAs for epithelial morphogenesis (Harris et al. 2006). The deletion of microRNAs miR-17 and miR-92, which together form a cluster in mice, exhibited early embryonic or post-natal lethality, characterized by severely hypoplastic lungs (Carraro et al. 2009).

Given the emerging importance of microRNA in organ development, including the early development of the lung, it has been hypothesized that microRNAs also have a functional role in late lung development, especially during secondary septation. To investigate the above hypothesis, the following aims were explored.

The specific aims of this study were:

1. Screening of microRNA expression during normal late lung development;

2. Screening of microRNA expression during pathological late lung development;

3. Investigate whether microRNAs have a functional role during pathological late lung development;

4. Associate specific microRNAs with candidate mRNA targets;

5. To test whether restoration of microRNA levels can be accomplished *in vivo*;

3 Materials and methods

3.1 Materials

3.1.1 Technical equipment

Equipment	**Manufacturer**
Bacterial culture incubator	Heraeus, Germany
Cell culture incubator HERAcell 150i	Thermo scientific, USA
Cell culture working bench	Thermo Scientific, USA
Centro LB microplate luminometer	Berthold, Germany
Countess® cell counter	Invitrogen, UK
Developing machine X omat 2000	Kodak, USA
Electrophoresis chambers	Bio-Rad, USA
Gel blotting paper	Bioscience, Germany
Inolab® pH meter	WTW, Germany
Isoplate™B&W 96-well plate	PerkinElmer, USA
Light microscope	Leica, Germany
MicroAmp® 8-tube strip	Applied Biosysystems, USA
Microcentrifuge tubes:0.5, 1.5, 2ml	Eppendorf, Germany
Mini shaker	VWR, USA
Mini Trans-Blot® western blot chambers	Bio-Rad, USA
Minispin® centrifuge	Eppendorf, Germany
MS-100 thermo shaker	Universal Labortechnik, Germany
Nanodrop® ND 1000	Peqlab, Germany
Nanozoomer XR C12000	Hamamatsu, Japan
Nylon net filters, 20µm	Millipore, USA
PeqSTAR 96 universal gardient thermocycler	Peqlab, USA
Petri dishes	Greiner Bio-one, Germany
Pipetboy	Eppendorf, Germany
Pipetmans: P10, P20, P100, P200, P1000	Gilson, France

Pipetman filter tips:10, 20, 100, 200, 1000 µl	Greiner Bio-One, Germany
Refrigerated microcentrifuge CT15RE	VWR, USA
Serological pipettes: 5, 10, 25, 50 ml	Falcon, USA
StepOne Plus™ Real-Time PCR system	Applied Biosystems, USA
Test tubes: 15, 50 ml	Greiner Bio-One, Germany
Tissue culture dish 100 mm	Greiner Bio-One, Germany
Tissue culture flask 250 ml	Greiner Bio-One, Germany
Tissue culture plates: 6-, 12-, 48- and 96-well	Greiner Bio-One, Germany
Tranfer membrane nitrocellulose	Bio-Rad, USA

3.1.2 Chemicals and reagents

2-Propanol	Merck, Germany
Agarose	Promega, Germany
Ammonium chloride	Sigma-Aldrich, Germany
Ammonium persulfate	Promega, Germany
Ampicillin sodium salt	Sigma-Aldrich, Germany
Antagomirs-LNA	Exiqon, Denmark
Bovine serum albumin	Sigma-Aldrich, Germany
Complete™Protease inhibitor	Roche, Germany
dNTP mix	Promega, USA
DTT	Promega, USA
Dual-Luciferase® reporter assay system	Promega, USA
Dulbecco's modified Eagle's medium	Gibco BRL, Germany
Dulbecco's modified Eagle's medium, high glucose	Gibco BRL, Germany
Dulbecco's phosphate buffered saline	PAA Laboratories, Austria

Dulbecco's phosphate buffered saline, 1×	PAA Laboratories, Austria
EDTA	Sigma-Aldrich, Germany
EGTA	Sigma-Aldrich, Germany
Ethanol 70%	SAV-LP, Germany
Ethanol 99%	J.T. Baker Mallinckrodt Baker B.V., The Netherlands
Ethanol absolute	Riedel de Hän, Germany
Ethidium bromide	Promega, USA
Fetal calf serum	PAA Laboratories, Austria
Giemsa's azur eosin methylene blue solution	Merck, Germany
Glycerol	Carl Roth, Germany
Glycine	Carl Roth, Germany
Glycol methacrylate	Heareus Kulzer, Germany
Hank's balanced salt solution	PAA Laboratories, Austria
HEPES	PAA Laboratories, Austria
Hydrochloric acid	Sigma-Aldrich, Germany
Isoflurane	CP-Pharma, Germany
Lipofectamine™ 2000	Invitrogen, UK
Luria-Bertani medium	Invitrogen, UK
Magnesium chloride	Sigma-Aldrich, Germany
Magnesium chloride, 25mM	Applied Biosystems, USA
May-Gruenwald's eosin-methylene blue solution	Merck, Germany
β-mercaptoethanol	Sigma-Aldrich, Germany
Methanol	Fluka, Germany
MuLV reverse transcriptase	Applied Biosystems, USA
Non-fat dry milk	Carl Roth, Germany
Nuclease free water	Ambion, USA
Opti-MEM® medium	Gibco BRL, Germany
Osmium tetroxide	Sigma-Aldrich, Germany
Passive lysis buffer	Promega, USA
PCR buffer II, 10×	Applied Biosystems, USA

Penicillin/streptomycin	PAA Laboratories, Austria
Potassium bicarbonate	Sigma-Aldrich, USA
PrecisionPlus Protein™standards	Bio-Rad, USA
Proteinase K	Promega, USA
QIAquick gel extraction kit	Qiagen, The Netherlands
QIAquick PCR purification kit	Qiagen, The Netherlands
Quick start™Bradford dye reagent	Bio-Rad, USA
Random hexamers	Applied Biosystems, USA
RIPA buffer	Thermo Scientific, USA
RNase inhibitor	Applied Biosystems, USA
Rotiphorese Gel 30 acrylamide/bisacrylamide mix	Carl Roth, Germany
SDS, 10% solution	Promega, USA
SDS, powder	Carl Roth, Germany
Select agar	Sigma-Aldrich, Germany
Sodium acetate	Sigma-Aldrich, Germany
Sodium cacodylate trihydrate	Sigma-Aldrich, Germany
Sodium chloride	Merck, Germany
Sodium orthovanadate	Sigma-Aldrich, Germany
Sodium phosphate	Sigma-Aldrich, Germany
Sodium sulfate	Merck, Germany
Supersignal® West Femto chemiluminescent substrate	Thermo scientific, USA
TEMED	Bio-Rad, USA
TGF-β1	R&D Systems, USA
Tris	Carl Roth, Germany
Triton X-100	Promega, USA
TRIzol® reagent	Ambion, USA
Trypan blue	Fluka, Germany
TurboFect reagent	Thermo scientific, USA
Tween® 20	Sigma-Aldrich, Germany
Uranyl acetate	Serva, France

3.1.3 Cell lines

NIH/3T3 fibroblast cell line, Invitrogen, UK

3.2 Methods

3.2.1 NIH/3T3 cell culture

NIH/3T3 mouse embryonic cell line was cultured in culture flasks using Dulbecco's modified Eagle's medium (DMEM) containing supplemental 10% fetal bovine serum (FBS), at 37 ºC with 5% CO_2 and 95% humidity. When cells reached 70-80% confluency, were subcultured (after being washed using phosphate-buffered saline – PBS) followed by incubation with 3 ml Trypsin-EDTA for 5 min at 37 ºC. The next step was to inhibit the activity of the enzyme by using 7 ml of culture medium with FBS. The cell suspension was diluted 1:3 in medium plus the FBS and it was passed into a new cell culture flask.

3.2.2 Culture of primary fibroblasts

Primary mouse lung fibroblasts were isolated using a modified protocol published by Seluanov and collaborators (Seluanov et al. 2010). Female adult C57BL/6J mice were sacrificed using isofluorane. The anterior abdomen was opened by midline incision using with sterile scissors. The lungs were perfused using PBS, after puncturing the left atrium and injected through the right ventricle. The lungs were removed, were transferred to a cell culture dish containing 10 ml of cold isolation medium and were cut into small pieces using sterile scissors. The pieces were transferred to a 50 ml Falcon containing pre-warmed 2 mg/ml collagenase type I, and left incubating at 37 ºC for 45 min. The resulting suspension was filtered through a 40-µm cell strainer. The filtrate was then centrifuged at 400 g for 8 min at 4 ºC and the pellet was re-suspended in 10 ml of growth medium. The solution was centrifuged again at 400 g for 8 min at 4 ºC (washing). The pellet was suspended in 10 ml of growth medium, and the suspension was added to a new culture flask.

Isolation medium	**Growth medium**
High glucose DMEM	High glucose DMEM
20% FBS	10% FBS
1% penicillin/streptomycin	1% penicillin/streptomycin

3.2.2.1 Treatment of primary fibroblasts

Primary lung fibroblasts were seeded on a 6-well plate at a density of 10^6 cells/well. Each well was treated with 5 ng/ml of TGF-β1 for 6 or 24 h. The use of SB431542 (10 nM) inhibited the TGF-β signaling; the inhibitor was added to the media at the same time as the transfection reagents.

3.2.2.2 Transfection of microRNA mimics and short interfering RNA

The TurboFect transfection reagent (Thermo Scientific) was used to transiently transfect primary mouse lung fibroblasts with microRNA mimics or siRNA. The cells were seeded 48 h prior to transfection into a 6-well plate until they reach 50% of confluency. In order to transfect the cells, the siRNA or the microRNA mimics were added to a solution containing 4 µl of TurboFect and 50 µl of Opti-MEM® serum free medium, for 20 min in RT. The solution was added to each well. The final concentration of microRNA mimics or control was 40 nM and the concentration of siRNA was 100 nM. Cells were cultured for 24 h under normal cell culture conditions or exposed to 5 ng/ml TGF-β1 after 24 h for additional 6- h.

3.2.3 Dual luciferase reporter assay

The dual luciferase assay, containing both the firefly luciferase and *Renilla* luciferase reporters, was used in order to assess TGF-β signaling. The NIH/3T3 cells were transfected with the firefly luciferase construct and with pRSL-SV40 that constitutively expresses *Renilla* luciferase, using TurboFect, followed by a 6 h transfection in Opti-MEM®. The cells were subsequently transfected with 40 nM of either control or mimic, using also TurboFect, and were incubated for 6 h in Opti-

MEM®, after which medium was exchanged for DMEM with 10% FBS, and then cells were stimulated with TGF-β or vehicle. The dual luciferase ratio (DLR) was calculated from luminescence units generated by firefly luciferase and were normalized by units generated by *Renilla* luciferase.

3.2.4 Plasmid construction and transfection

The full length of *Smad7* 3 prime UTR containing the predicted miR-15 family binding site was amplified by PCR from genomic mouse DNA and subcloned into the pmirGLO Dual luciferase microRNA target expression vector (Promega) between the *SacI* and *XbaI* sites. The method has been described in detail previously (Nicolas 2011). The orientation and sequence of the fragment in the luciferase reporter were confirmed by sequencing and enzyme digestion. Transient transfections were performed using Turbofect, followed by a 6 h transfection in Opti-MEM®. The luciferase reporter construct was transfected into NIH/3T3 cells (100 nM) along with *Renilla* luciferase control reporter vector and 40 nM of either control or microRNA mimic. The dual luciferase ratio (DLR) was calculated from luminescence units generated by firefly luciferase and were normalized by units generated by *Renilla* luciferase.

3.2.5 Gene expression analysis

3.2.5.1 RNA isolation from cells and lung tissue

Total RNA was isolated from ~ 50 mg of lung tissue using 1 ml of QIAzol® lysis reagent per 100 mg tissue. The lung tissue was homogenized by using Precellys® 25 homogenizer. Subsequently, 0.3 ml of chloroform was used and the samples were centrifuged at 12000 g for 15 min at 4 ºC. Following centrifugation, the aqueous phase supernatant solution was transferred to 1.5 ml tube, and samples were mixed with 0.5 ml of 100% ethanol per 1 ml of QIAzol® lysis reagent, and left for 5 min at RT. The samples were added to an RNA column (miRNeasy kit – Qiagen) and were centrifuged at 10000 rpm for 2 min. The flow through was removed and the column was washed using buffer I and II (miRNeasy kit). 50 µl of nuclease free water were

added to each column, and the flow through containing the total RNA was measured by using NanoDrop® ND 1000 spectrophotometer.

Total RNA containing microRNAs from cells in culture was isolated using the same kit mentioned above according to the manufacturer's instructions. The quantity and the quality of the RNA was measured by using NanoDrop® ND 1000.

3.2.5.2 MicroRNA microarrays

For gene expression and microRNA expression arrays, lung homogenates derived from pups maintained under normoxic or hyperoxic conditions, were used for total RNA extraction. The microarrays comparisons were performed by IMGM Laboratories (Martinsfreid, Germany) using Agilent mouse microRNA microarrays (8×60K format) in combination with one-color based hybridization protocol. Signals on the microarrays were detected using the Agilent DNA Microarray Scanner and GeneSpring GX12 analysis software was used to normalize the raw data.

3.2.5.3 cDNA synthesis (mRNA)

The reverse transcription was performed on 1 μg of total RNA using MuLV reverse transcriptase and random hexamers (oligodeoxyribonucleotides). First, 20 μl of RNA was denatured at 70 ºC for 10 min, and supplemented with 20 μl of reverse transcription mixture. The mixture was incubated at 21 ºC for 10 min and it was followed by an RNA synthesis step at 43 ºC for 75 min. The final step of the reaction included the inactivation of the MuLV reverse transcriptase at 99 ºC. The reverse transcription mixture is shown below:

Reverse transcription mixture	**Volume**
10× PCR buffer II	4 μl
25 mM $MgCl_2$	8 μl
H_2O	1 μl
Random hexamers	2 μl
RNase inhibitor	1 μl
10 nM dNTP mix	2 μl
MuLV reverse transcriptase	2 μl
Total volume	20 μl

3.2.5.4 cDNA synthesis (microRNAs)

The reverse transcription was performed on 1 µg of total RNA using miScript II (Qiagen). A reverse transcription master mix was prepared that contains all the components for the first-strand cDNA synthesis except template RNA. Starting with cDNA synthesis, the RNA was denatured for 10 min, and supplemented with the master mix. The solution was incubated for 60 min at 37 ºC, followed by the inactivation of reverse transcriptase at 95 ºC. The reverse transcription master mix is shown below:

Reverse transcription mixture	**Volume**
5× miscript buffer	4 µl
10× nucleic mix	2 µl
H_2O	variable
Reverse transcriptase	2 µl
Template RNA	variable
Total volume	20 µl

3.2.5.5 Real-time quantitative PCR (mRNA)

The analysis of the gene expression was performed by real-time quantitative polymerase chain reaction (qPCR) using Platinum® SYBR® Green qPCR Supermix UDG kit and a StepOnePlus™ Real-Time PCR system. Primer pairs specific to the target mRNA were designed using Primer-BLAST software (http://www.ncbi.nlm.nih.gov/tools/primer-blast). The primers used are listed below:

Gene	**Species**	**Forward and reverse primer sequences**
Ctgf	*mouse*	5´- GGGCCTCTTCTGCGATTTC- 3´ 5´- ATCCAGGCAAGTGCATTGGTA- 3´
Smad7	*mouse*	5´- GGCCGGATCTCAGGCATTC - 3´ 5´-TTGGGTATCTGGAGTAAGGAGG -3´

α-SMA	*mouse*	5´- GTCCCAGACATCAGGGAGTAA – 3´ 5´- TCGGATACTTCAGCGTCAGGA – 3´
Hprt1	*mouse*	5´- TCAGTCAACGGGGGACATAAA – 3´ 5´- GGGGCTGTACTGCTTAACCAG – 3´

The thermal cycling steps for the real-time PCR were as follows: 50º C for 2-min, 95 ºC for 5 min, 35-40 cycles of 95 ºC for 5 s, 72 ºC for 30 s. At the end of the program, the samples were subjected to melting curve analysis in order to exclude the possibility of primer/dimer formation. *Hprt* gene was used as a reference gene for the reactions. The expression of the genes was assessed with the comparative Ct method (ΔCt) and was calculated with the formula: $\Delta Ct = Ct_{\text{Reference gene}} - Ct_{\text{target gene}}$

3.2.6 Protein expression analysis

3.2.6.1 Protein isolation

The procedure of protein isolation was carried out carefully on ice in order to prevent protein degradation. The protein lysis buffer was supplemented with sodium orthovanadate and 1 mM Complete™ protease inhibitor mixture, right before its use. Next, 250 µl of protein lysis buffer was added to the NIH/3T3 or the primary fibroblasts seeded on 6-well plates, and cells were collected using a cell scraper into 1.5 ml tubes and were incubated for 30/45 min on ice. The tubes were centrifuged at 12000 rpm for 15 min at 4 ºC and the supernatant was transferred to new 1.5 ml tubes. In order to measure the protein concentration, samples were diluted 1:10 in nuclease free water and 10 µl were transferred into a 96-well plate. On the same plate, a series of bovine serum albumin (BSA) were also present, included as standards. On top of the 10 µl, 200 ml of Quick Start™ Bradford dye reagent was added to each well and the absorbance was measured at a 570 nm wavelength using VersaMax plate reader. The concentrations of the proteins were calculated for each sample using the standard curve.

Protein lysis buffer
150 mM NaCl
1 mM EDTA
1 mM EGTA
0.5% Igepal® CA-630
20 M Tris-Cl, PH 7.5

3.2.6.2 Protein electrophoresis and western blot

The protein samples were mixed with 2× loading buffer and resolved by sodium sulfate polyacrylamide gel electrophoresis at a constant 110 mV, in running buffer. The proteins were blotted onto a nitrocellulose membrane at 110 mV for 1 h in blotting buffer. The membrane was washed with washing buffer and incubated for 45 min in protein blocking solution at RT. The primary antibody was diluted in blocking buffer, and the membrane was soaked in the solution overnight at 4 ºC. The primary antibodies that were used in this study are listed below. The membrane was washed using a washing buffer, and the horseradish peroxidase-conjugated secondary antibody diluted in blocking solution was added. The membrane was incubated in solution at RT for 1 h. Thereafter, the membrane was washed and was incubated in SuperSignal® West Femto chemiluminescent substrate for 5 min. The protein bands were visualized using a LAS-4000 luminescent image analyzer. The antibodies that were used are listed below:

Antibody	**Dilution**	**Company**	**Catalog number**
Anti–β-ACTIN	1:1000	Cell Signaling Technology, USA	4967L
Anti-SMAD7	1:500	Santa Cruz Biotechnology, USA	Sc365846
Anti-pSMAD2	1:1000	Cell Signaling Technology, USA	3101
Anti-SMAD2/3	1:1000	Cell Signaling Technology, USA	3102
Anti-α-SMA	1:1000	Abcam	5694

10% Resolving gel
10% acrylamide/bisacrylamide mixture

375 mM Tris-Cl, pH 8.8

0.05% SDS

0.05% APS

0.065% TEMED

10× Sample buffer
650 mM Tris-Cl, PH 6.8

1 mM EDTA

50% glycerol

0.3% bromophenol blue

9% β-mercaptoethanol

Running buffer

250 mM Tris-Cl, pH 8.3

2.5 M glycine

1% SDS

Washing buffer

1× PBS, pH 7.2

0.1% Tween® 20

Stacking gel

5% acrylamide/bisacrylamide mixture

125 mM Tris-Cl, pH 6.8

0.05% SDS

0.05% APS

0.065% TEMED

Blocking buffer

1× PBS, pH 7.2

0.1% Tween® 20

5% non-fat dry milk

Blotting buffer

25 mM Tris-Cl, pH 8.3

192 mM glycine

20% methanol

3.2.7 Animal experiments

3.2.7.1 The mouse model of bronchopulmonary dysplasia

All animal experiments and procedures were approved by Regierungpräsidium Darmstadt (approvals B2/351 and B2/1002). There was an extensive arrest of alveolarization in mouse pups after exposure to normobaric hyperoxia (85% O_2). This model has been described in previous studies (Kumarasamy et al. 2009) where there was an extended arrest of lung development in response to hyperoxia. Both the normoxia (21% O_2) and the hyperoxia (85% O_2) groups were divided into two subgroups and were treated with two intraperitoneal (ip) injections of either control mimic (Scr) or with a mixture of miR-15b and miR-497 LNA-antagomirs at a dose of 10 mg/kg dissolved in water, on day 1 and 3; Nursing dams were exchanged every 24 h between normoxia and hyperoxia in order to minimize oxygen toxicity. Dams and pups received food *ad libitum* and were maintained on 12 h light dark cycle. Pups were sacrificed on the fourteenth day after birth (P14) by the use of isofluorane followed by lung extraction.

3.2.7.2 Lung stereology

The American Thoracic Society/European Respiratory has recently published specific recommendations for the assessment of lung structure (Hsia et al. 2010). The mouse lungs were fixed via a tracheal cannula at a stable hydrostatic pressure of 20 cmH_2O, using a solution containing 1.5% (wt/vol) paraformaldehyde, 1.5 % (wt/vol) glutaraldehyde in 150 mM HEPES, for 24 h at 4 °C. The lung volume was measured by water displacement and the results were confirmed by applying Cavalieri's principle (Tschanz et al. 2011). Following a systematic uniform randomization (SUR) rule, the tissue blocks were embedded in glycol methacrylate (Technovit 7100) in order to eliminate the standard error derived from tissue shrinkage. Slices were cut from each block (thickness of 2 μm), mounted on slides and were stained using Richardson's stain; every first and third section were chosen for analysis and were digitally scanned using the NanoZoomerXR digital slide scanner. The lung structure analysis was carried out using the most updated version of Visiopharm NewCast

stereology software (VIS 4.5.3). The stereological assessment of surface density, mean linear intercept and septal thickness was carried out with a magnification of 20×; initially a test grid with counting points (crosses) was used to count on microscopic digital images generated by SUR. As depicted in Figure 3-1 A, the test points fall either on airspaces $P(_A)$ or on septal tissue $P(_{sep})$. This allows an estimation of the volume fraction of airspaces Vv(air,par) and septal tissue Vv(sep,par) within parenchyma. In the next step, linear intercepts were measured on the same digital images by using a line segment of approximately 70 μm that was projected on the image with a random orientation (Fig 3-1 B). A measurement was performed each time the line intersected an alveolar surface (marked as I) and also when the two endpoints of the line were within the parenchyma, taken as points (marked as P). After counting 60 to 100 fields and obtaining around 150 count points and intersections, the mean linear intercept (MLI) was obtained; this is the mean free distance in the airspaces in the lung (Knudsen et al. 2010). The second important parameter that can be calculated by using the above parameters is septal thickness (St).

In order to define the total alveoli number in the mouse lungs, the physical dissector methodology was used. As depicted in Figure 3-1 C and D, a counting frame is projected on the digital images, taken from the first and the third sections in a consecutive series of serial sections, each of 2 μm thickness. When there is an alveolar opening open in one section and closed in the other section or *vice versa*, this is counted as a bridge (marked as B). After counting 60 to 100 fields (marked as M), the number of bridges is used in a formula to obtain the total number of alveoli.

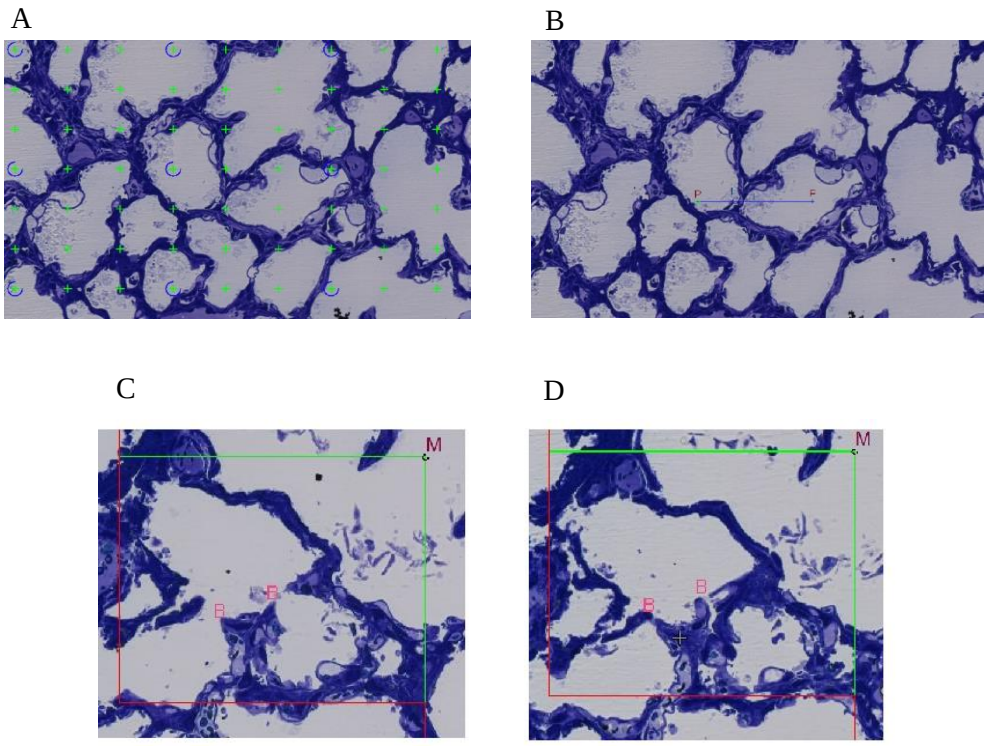

Figure 3-1 Stereological analysis of neonatal mouse lungs.

A: An example of a point grid projected on the digital image from a mouse lung at P14, that was exposed to hyperoxia. When the crosses fall on airspaces, are counted as $P(_A)$ or when crosses fall on septa are counted as $P(_{sep})$. These counts give the first estimation of volume fractions within parenchyma. B: a system consisting of a line segment with a length of 72.49 µm. When the endpoints of the line fall within the parenchyma are counted (P) and also the number of intersections of the line with the alveolar surface (I). C and D: A counting frame is projected over the image in both fields of view. Alveolar bridges (B) are counted in every field (M).

3.3 Statistical analyses

Values are presented as mean ± SEM. Statistical comparisons between means of two groups were performed using unpaired Student's t-tests. For multiple comparisons, statistical analysis was performed using 1-way ANOVA followed by Bonferroni post hoc test. P values are considered significant below 0.05. The software used for the statistical calculations are GraphPad/Prism (GraphPad Prism version 6.00 for Windows, GraphPad Software, La Jolla California USA, www.graphpad.com) and R(http://cran.r-project.org/).

4 Results

4.1 Secondary septation peaks at P5.5 in mice

In order to investigate the post-natal (P) time point that secondary septation peaks, mouse lungs were extracted in different time points and were stained, as depicted in Figure 4-1. Postnatal 2.5 and P3.5 represent stages before the peak of secondary septation, P5.5 represents the peak of secondary septation and P14.5 represents the stage in which the alveolarization is almost complete. The lung structure looks more complicated with definitive alveoli already being formed.

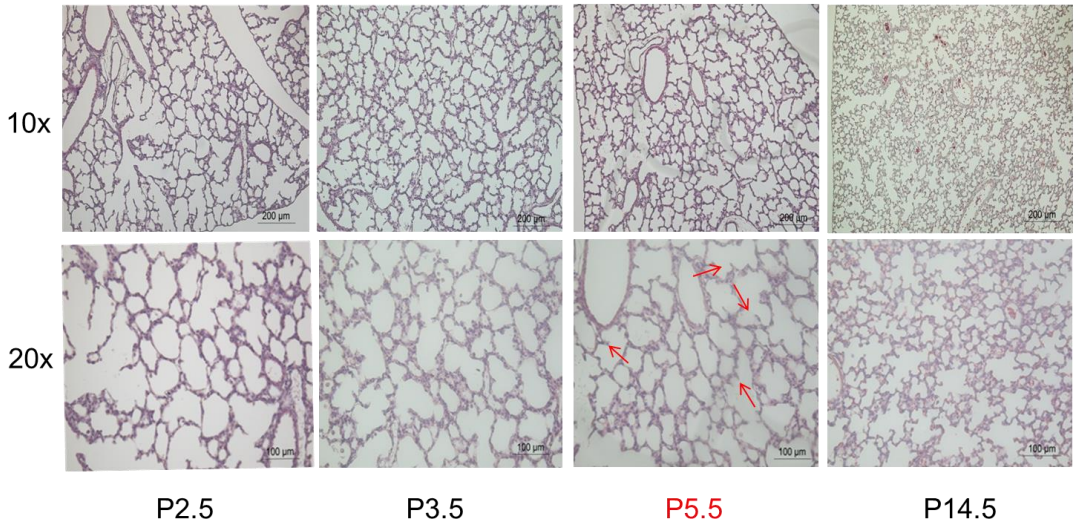

Figure 4-1 H&E sections representing the stages before, during and after secondary septation. The red arrows in P5.5 point on the newly-formed secondary septa.

The above finding indicates the most important time points where the study can focus on. The peak of septation takes place within six days after birth and is almost complete on P14.5. Studies have reported that alveolarization can continue until adulthood (Mund et al. 2008).

4.2 Expression analysis of microRNAs under normoxic conditions

As an initial screening, an unbiased screen by microarray of microRNA expression was performed on lung tissue from pups under normoxic conditions. The time points that were chosen for the screening were indicated above (P2.5, P3.5, P5.5, P14.5). The microRNAs that were distinguished by a high level of expression in all four time points were miR-15b, miR-5097, miR-136, miR-541, miR-18a, miR-210 and miR-154. MiR-127 was the microRNA with the most dramatic changes between different time points. Baskaran et al. has reported that miR-127 showed the highest expression just before and after birth in the lungs extracted from rats (Bhaskaran et al. 2009). The total number of microRNAs that had at least one significant change in the expression level between the four time points was 67; the microRNAs are presented in Figure 4-2.

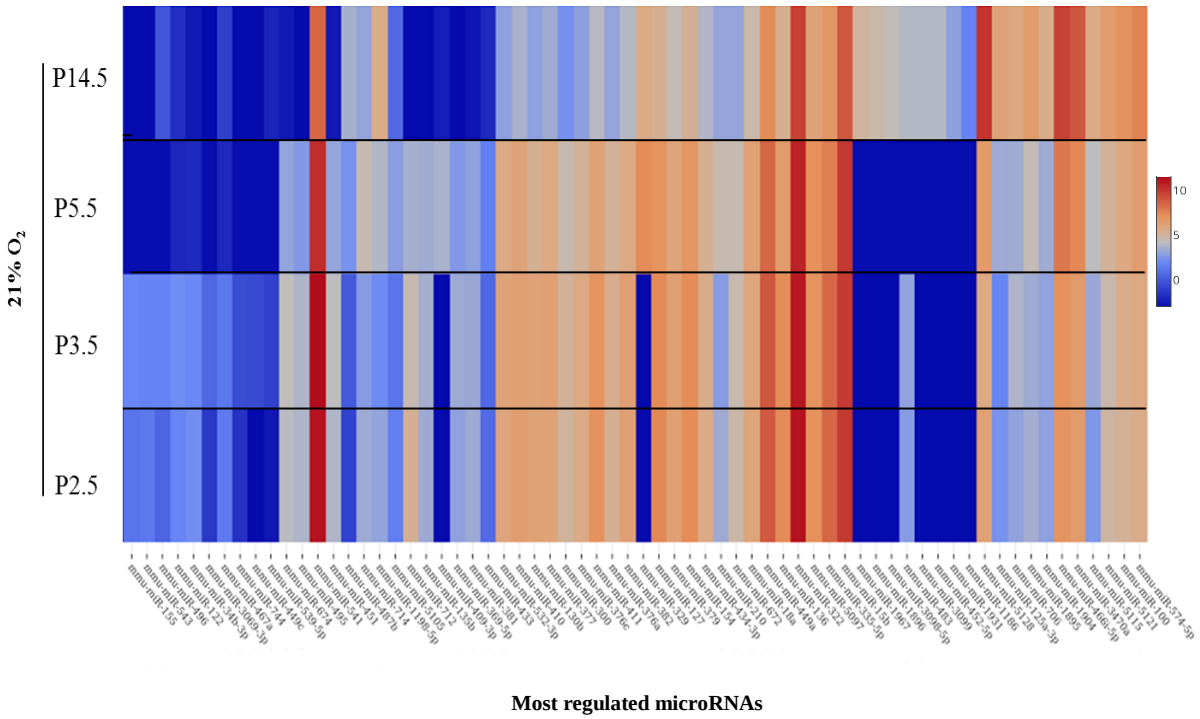

Figure 4-2 Expression patterns of microRNAs during late lung development using a color heat map.

Data were subjected to significant analysis of microarrays (SAM). Every row represents a time point and every column a microRNA. Each value of expression is the average of 4 samples and is $\log_2$ transformed. The red represents high intensity values, the blue low intensity values.

4.3 Expression analysis of microRNAs after exposure to hyperoxia

Later on, an unbiased screen by microarray of microRNA expression was performed on lung tissue from pups exposed to 21% O_2 and 85% O_2 during the four time points. The data clearly demonstrate that hyperoxia, as employed in the BPD model, has a dramatic and rapid impact on microRNA expression, with possible consequences for the development of the lung. In this study, a total number of 55 microRNAs showed a significant deregulation indicating a possible role in a pathological condition such as BPD (Fig 4-3).

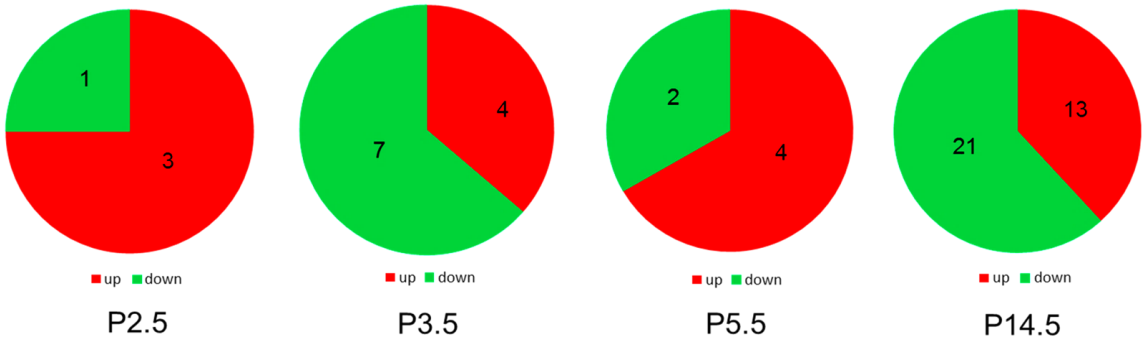

Figure 4-3 Whole lung homogenates were screened for changes in microRNA expression after exposing mouse pups to hyperoxia. A total number of 55 microRNAs showed significant de-regulation in all four timepoints.

The microRNAs with an increased expression, compared to normoxia, are shown in Table 4-1. The up-regulated microRNAs were interesting candidates for further investigation; the reason is that antisense oligonucleotides are easy to be constructed and can be used to inhibit microRNA expression *in vivo*.

Table 4-1 MicroRNAs with increased expression after exposure to hyperoxia.
The values underneath the systematic name represent the P value after performing an unpaired Student's t-test between normoxia and hyperoxia groups (n=4).

P 2.5	P 3.5	P 5.5
miR-15b	miR-15b	miR-34a
(0.02)	(0.04)	(0.0003)
miR-363	miR-497	miR-135b
(0.02)	(0.001)	(<0.0001)
miR-200a*	miR-200a*	miR-34b-3p
(0.02)	(0.003)	(0.00027)
	miR-33	miR-29c
	(0.001)	(<0.0001)

4.4 The microRNA-15 family expression is deregulated after exposure to hyperoxia

In microarrays, miR-15b appeared in two time points; miR-497 appeared only once, but both molecules belong to the same microRNA family (Yue and Tigyi 2010) and for that reason were chosen as candidates for further investigation. The relationship between the expression levels of both microRNAs during hyperoxia was positive and strong, revealing a possible common pattern of transcription. Both microRNAs are transcribed from different chromosomes but the expression is highly correlated as depicted in Figure 4-4. This is an important finding indicating similar transcription patterns of molecules that belong to the same family.

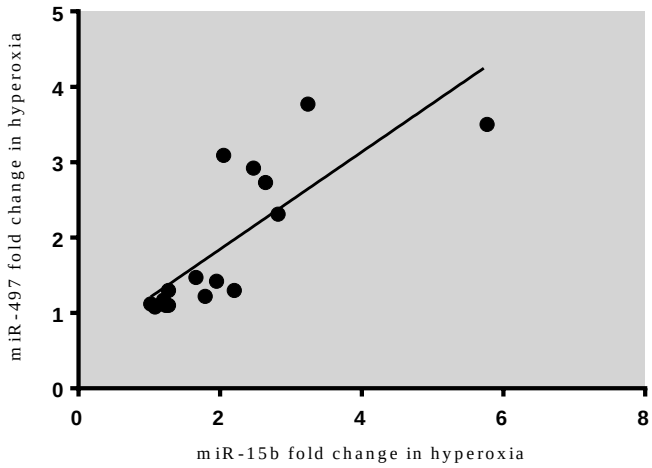

Figure 4-4 Analysis of the relationship between miR-15b and miR-497 expression after exposure to hyperoxia.

Correlation of expression fold changes of miR-15b and miR-497, under hyperoxic conditions, was assessed (n=4, per group). Proportion of variability was determined by calculating the Pearson coefficient of determination (R^2).

Mir-15 family expression, under normoxic and hyperoxic conditions, was validated by real time RT-PCR. The expression analysis included all six members of the miR-15 family; all members were initially up-regulated after exposure to hyperoxia with miR-15b and miR-497 being the most up-regulated (Fig 4-5, B and C). During the peak of secondary septation, the expression levels of most of the members were normalized to levels observed under normoxic conditions, and then were elevated again in P14.5, as depicted in Figure 4-5.

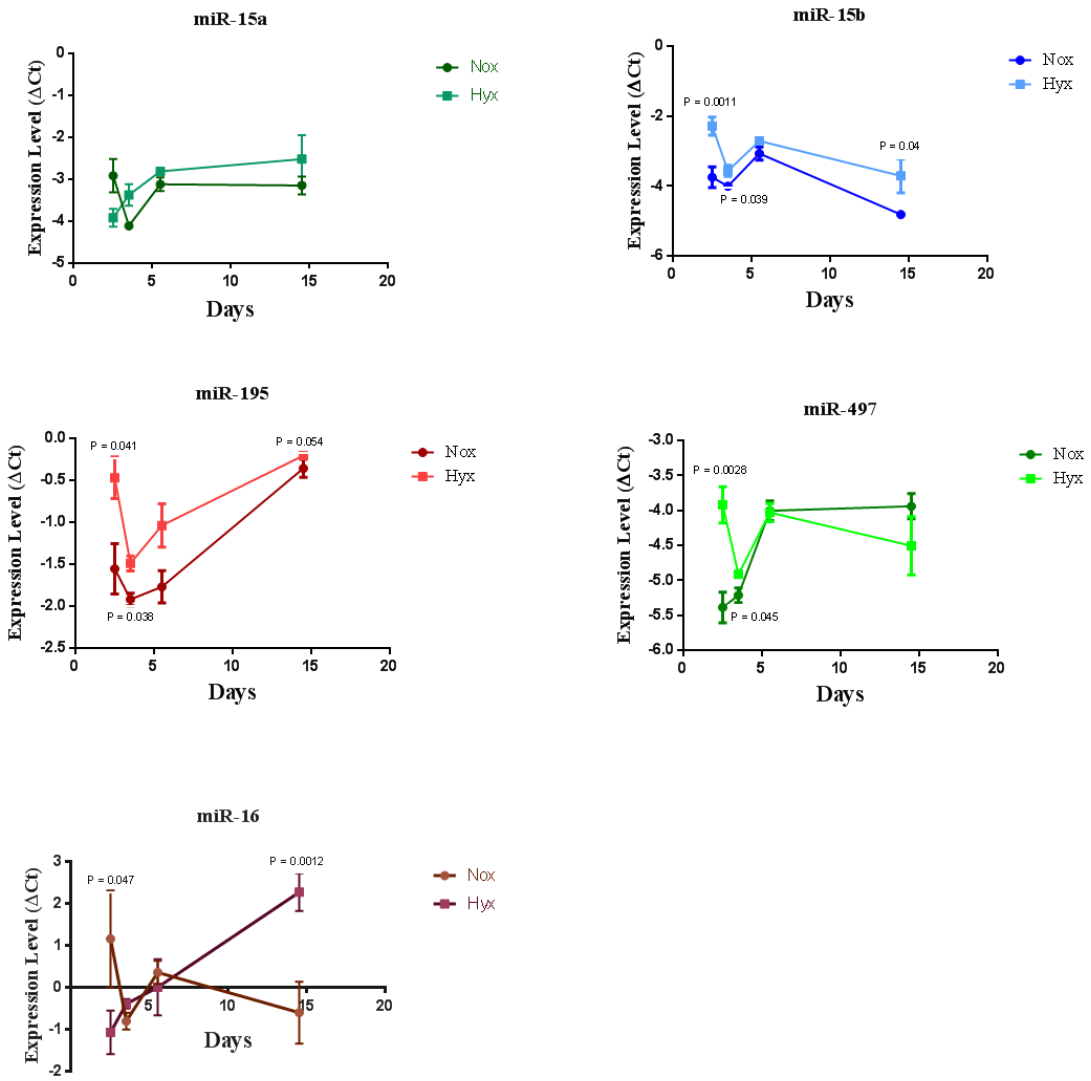

Figure 4-5 Differential expression of the microRNA-15 members under normoxia *versus* hyperoxia.

Expression levels of miR-15 family members were assessed by real time RT-PCR in the mouse lungs (n=6, per group) in normoxia *versus* hyperoxia. The five members share the same 'seed' sequence although are transcribed from different gene clusters. Data are expressed as mean ± SEM. Nox, normoxia; Hyx, hyperoxia. P values were determined by 1-way ANOVA with a Bonferroni post hoc test.

In P2.5, miR-15b and miR-497 had a significant difference in expression levels between normoxia and hyperoxia and were interesting candidates for further investigation.

4.5 The microRNA-15 family expression in primary lung cells

The next step was to identify in which cell-type miR-15b and miR-497 were mostly expressed. For that reason five major cell-types in the lung (Crapo et al. 1982) were used for the microRNA screening. As depicted in Figure 4-6, both miR-15b and miR-497 were expressed in a similar pattern in all cell-types derived from murine lungs, with no significant differences.

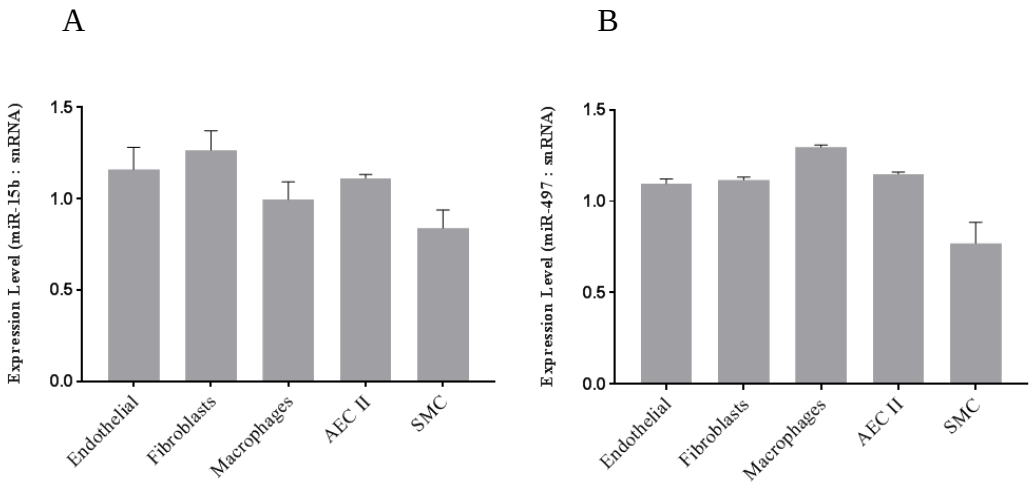

Figure 4-6 Expression of miR-15b and miR-497 in five primary lung cell types. Assessment of expression of miR-15 (A) and miR-497 (B) by real time RT-PCR (n=3, per cell-type). Data are expressed as mean ± SEM. snRNA, small nuclear RNA; AEC II, alveolar epithelial cells; SMC, smooth muscle cells. 1 – way ANOVA was used as a statistical comparison method.

The expression analysis suggests equal expression levels in every cell-type, however both miR-15b and miR-497 are transcribed from different chromosomes (Chamorro-Jorganes et al. 2011). It has been reported that the expression level of microRNAs depends on the expression of target mRNAs and can be tissue specific (Sood et al. 2006).

4.6 Target identification using computational methods

The functions of microRNAs are mediated by the ability to inhibit the expression of target mRNAs (Valencia-Sanchez et al. 2006). Identification of gene targets is a very important step in order to understand the role of microRNAs in gene

regulatory networks. One of the most common screening approaches for microRNA targets is *in silico*, based on computational algorithms comparing 'seed' sequences with conservational sites on the 3 prime untranslated regions (UTR) of genes (Friedman et al. 2009). Base pairing between microRNAs and targets, is analyzed and is based on many factors such as stable binding of 5 prime end of the microRNA, the thermodynamic binding of the two molecules through calculation of free energy (Watanabe et al. 2007).

In this study, for the identification of gene targets, the miRWalk algorithm (https://www.umm.uni-heidelberg.de) was used; this is a publicly available library of predicted and validated microRNA targets. The miRWalk algorithm lists all the possible targets obtained by using four major established algorithms such as Targetscan, miRanda, RNA22, miRDB. The illustration in Figure 4-7 represents the strategy designed to identify possible mRNA targets.

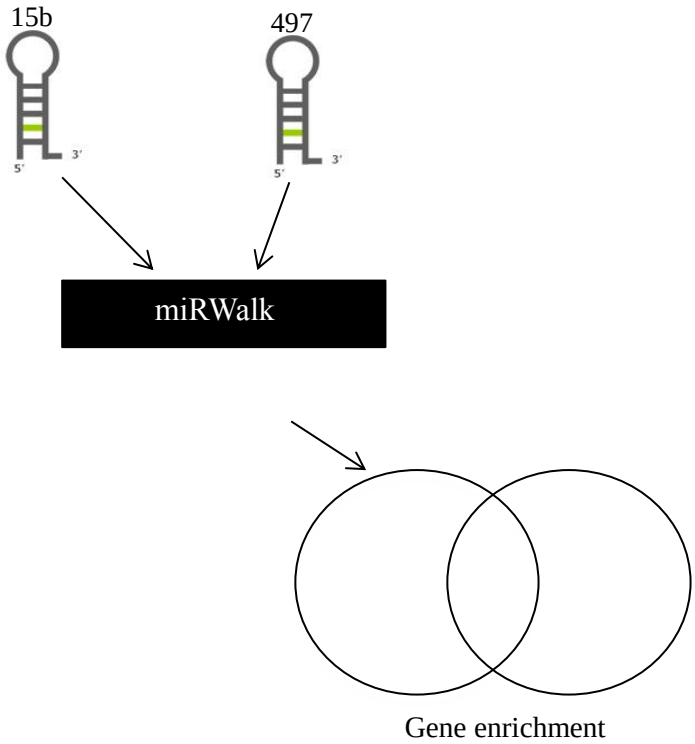

Figure 4-7 Illustration of the strategy being employed in order to identify microRNA targets.

MicroRNAs are checked by the 'seed' sequence, using the miRWalk algorithm. Some of the predicted targets of both microRNAs overlap which shows clearly that both miR-15b and miR-497 belong to the same family and share the same 'seed' sequence.

Computational prediction of microRNA targets usually returns many results. For this reason, all the predicted targets that resulted by using the four algorithms mentioned above, were enriched in order to eliminate inaccurate results. After enrichment using R software, 63 target genes overlapped from all four computational algorithms as shown in Figure 4-8.

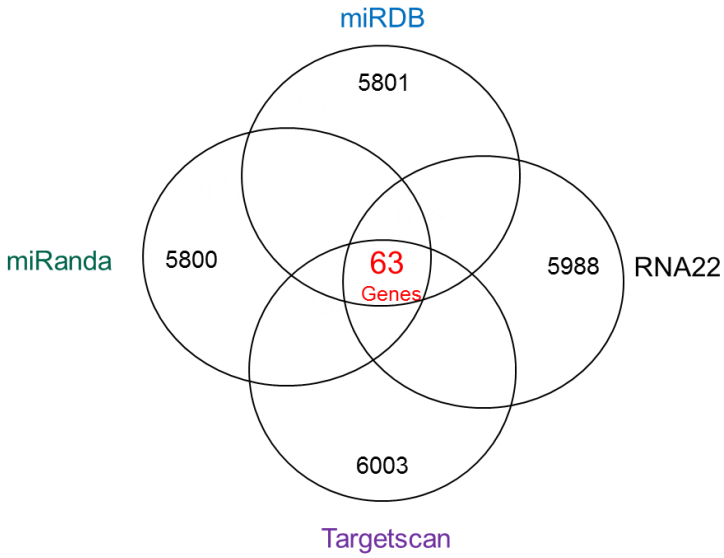

Figure 4-8 Gene target enrichment for the microRNA-15 family.
The target prediction algorithms that were employed returned hundreds of target candidates. In total 63 genes were common in all four algorithms.

MiRWalk microRNA prediction targets are depicted in Table 4-2 and are based on the probability of the microRNA-mRNA interaction. The table represents the gene target identification, the number of mRNA nucleotides that the microRNA binds, the miR 'seed' nucleotide sequence, the 3 prime UTR position and the P value showing the probability of this interaction. *Smad7*, a gene implicated in TGF-β signaling, is highlighted in the table as a target candidate.

Table 4-2 *In silico* analysis reveals miR-15 family target genes.

This is only a sample of candidate genes introduced as targets of miR-15 family. *Smad7* is highlighted as a candidate for the study. The table contains the miR, target gene, accession gene number, 'seed' sequence length, position, the region and the statistical P value.

mmu-miR-15b	Akap7	NM_018747	8	2930	UAGCAGCA	2937	3 UTR	0.0297
mmu-miR-15b	Smad7	NM_001042660	8	2941	UAGCAGCA	2948	3 UTR	0.0237
mmu-miR-15b	Hagh	NM_024284	8	1018	UAGCAGCA	1025	3 UTR	0.0026
mmu-miR-15b	Cldn12	NM_022890	8	1169	UAGCAGCA	1176	3 UTR	0.0389
mmu-miR-15b	Mnt	NM_010813	8	2557	UAGCAGCA	2564	3 UTR	0.0363
mmu-miR-15b	Sec24b	NM_207209	8	4071	UAGCAGCA	4078	3 UTR	0.0107
mmu-miR-15b	Mpl	NM_010823	8	1529	UAGCAGCA	1536	3 UTR	0.0435
mmu-miR-15b	Pcdh9	NM_001081377	8	4000	UAGCAGCA	4007	3 UTR	0.0273
mmu-miR-15b	Snf1lk	NM_010831	8	3159	UAGCAGCA	3166	3 UTR	0.0306
mmu-miR-15b	Ankrd58	NM_173779	8	1429	UAGCAGCA	1436	3 UTR	0.0078
mmu-miR-15b	Rwdd2b	NM_016924	8	1296	UAGCAGCA	1303	3 UTR	0.0161
mmu-miR-15b	Pnoc	NM_010932	8	1767	UAGCAGCA	1774	3 UTR	0.0187
mmu-miR-15b	Uqcc	NM_018888	8	1917	UAGCAGCA	1924	3 UTR	0.0229
mmu-miR-15b	Ttll6	NM_172799	8	3347	UAGCAGCA	3354	3 UTR	0.0082
mmu-miR-15b	Slc39a10	NM_172653	8	4444	UAGCAGCA	4451	3 UTR	0.0367

The *Smad7* gene plays an important role in TGF-β signaling and has a significant impact on organogenesis, cell cycle and development (Briones-Orta et al. 2011). As TGF-β has such an impact on late lung development and alveolarization (Alejandre-Alcazar et al. 2007), the relationship between miR-15 family and *Smad7* was further explored.

4.7 *Smad7* is a direct target of miR-15b

The validation of the computational prediction is important for understanding the biological significance of the microRNAs. In order to validate the hypothesis that *Smad7* is an actual target of miR-15 family, a luciferase reporter vector containing *Smad7* 3 prime UTR was used. Since fibroblasts are highly responsive to TGF-β, an experiment was performed using fibroblast NIH/3T3 cell lines. The NIH/3T3 cells were transfected using a miR-15b mimic, and a down-regulation of luciferase activity was observed, indicating that *Smad7* is a direct target of miR-15b (Fig 4-9).

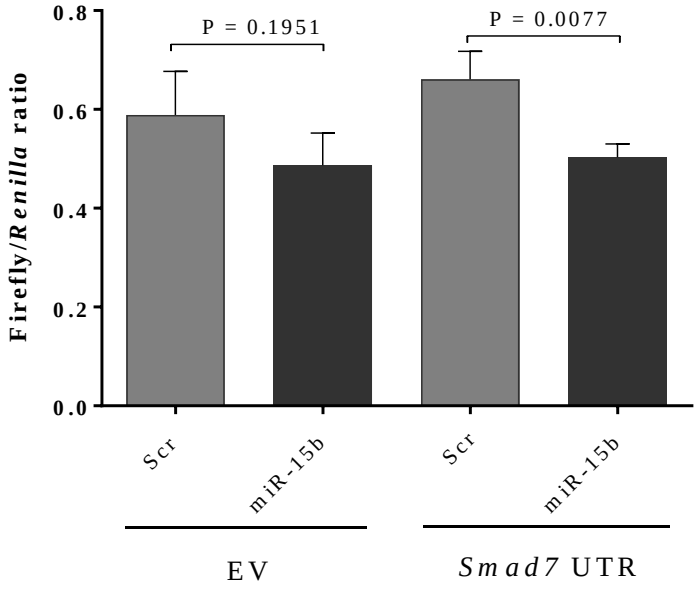

Figure 4-9 *Smad7* is a direct target of miR-15b.
NIH/3T3 cells were co-transfected with the 3 prime UTR *Smad7* vector or an empty vector (not containing a 3 prime UTR) and 40nM of miR-15b, or control mimic (Scr). The luciferase ratio was calculated from luminescence units generated by firefly and were normalized by units generated by *Renilla* luciferase. EV, empty vector; UTR, untraslated region. P values were determined by 1-way ANOVA with a Bonferroni post hoc test.

4.8 MiR-15b regulates TGF-β signaling through *Smad7*

After validating the direct binding of miR-15b to the *Smad7* 3 prime UTR, it was hypothesized that miR-15b has an impact on TGF-β signaling. To explore whether the miR-15b regulates the canonical TGF-β pathway, a CAGA luciferase reporter was used, with a Smad3-responsive element cloned into the pGL3-Basic vector, upstream of the luciferase gene. Overexpression of miR-15b, or transfection of *Smad7* siRNA, after TGF-β stimulation, led to an increase in luciferase activity in NIH/3T3 cells (Fig 4-10). These data support the fact that miR-15b has a similar effect as *Smad7* siRNA and leads to phosphorylation of SMAD2 and SMAD3 with a consequent increase of TGF-β signaling. This is the first *in vitro* evidence that the miR-15b induces the canonical TGF-β pathway. MiR-497 has an identical 'seed'

sequence as miR-15b, so it was hypothesized that the impact on TGF-β signaling is similar.

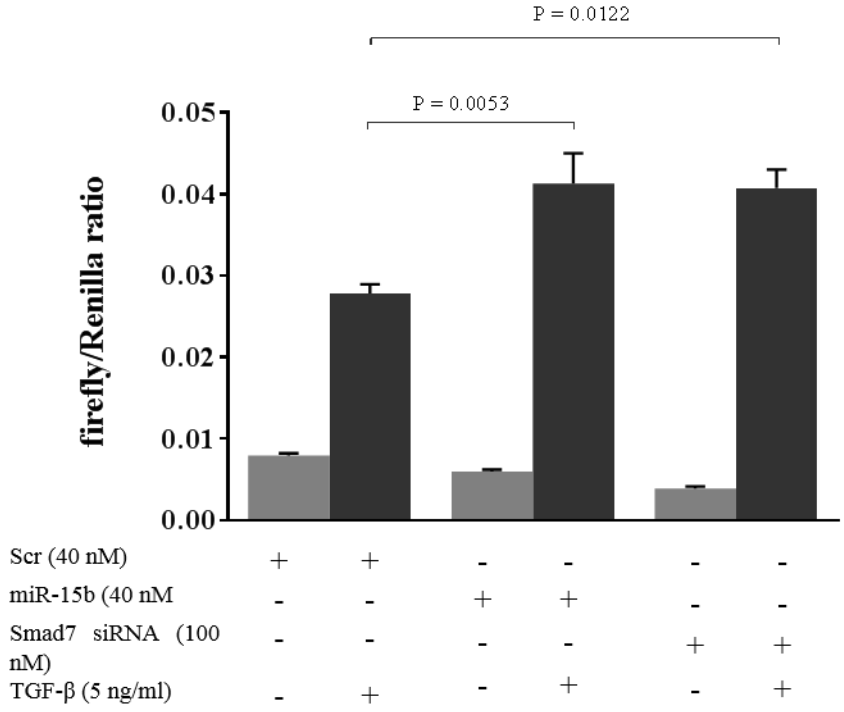

Figure 4-10 miR-15b overexpression modulates TGF-β signaling in NIH/3T3 cells.
NIH/3T3 cells were transfected either with 40 nM control or miR-15b mimic or 100 nM *Smad7* siRNA, and the effects on TGF-β signaling were assessed by using a Dual luciferase assay employing p(CAGA)$_9$-luc and pRL-SV40. The cells were stimulated either with vehicle or with 5 ng/ml of TGF-β for 24h. The data represent means ± SEM (n=6). P values were determined by 1-way ANOVA with a Bonferroni post hoc test.

Following the experimental validation that miR-15b modulates TGF-β signaling, the next step was to evaluate whether miR-15b and miR-497 overexpression has an impact on *Smad7* expression. For this reason, primary mouse lung fibroblasts were isolated and were transfected with microRNA mimics or control mimics. As depicted in Figure 4-11, overexpression of both miR-15b and miR-497 resulted in decreased *Smad7* mRNA (Fig 4-11 A) and protein levels (Fig 4-11 B). This finding also represents the identical functionality of both microRNAs.

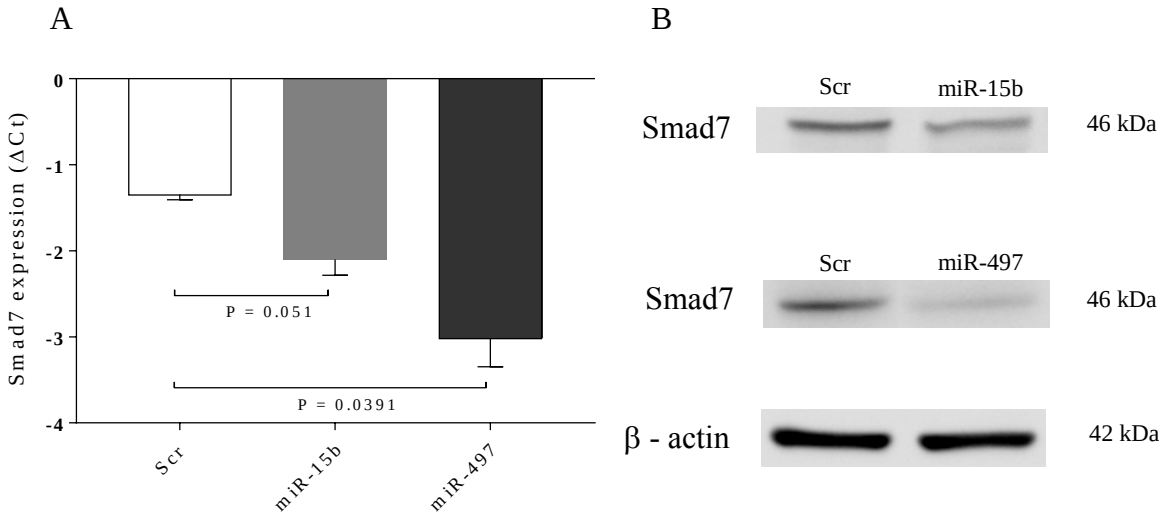

Figure 4-11 Impact of miR-15b and miR-497 overexpression on *Smad7* expression in primary lung fibroblasts.

Cells were transfected with 40 nM of control mimic (Scr), or miR-15b or miR-497 mimic for 24 h. (A) Expression analysis of the *Smad7* gene was assessed in primary fibroblasts after transfection, by real-time RT-PCR (n = 6, per group). (B) Total cellular protein was isolated, subjected to immunoblot with antibodies against SMAD7 and β-ACTIN. Data are expressed as mean ± SEM. P values were determined by using 1-way ANOVA with a Bonferroni post hoc test.

4.9 MiR-15b and miR-497 overexpression increases the differentiation of fibroblasts to myofibroblasts

Differentiation and plasticity in various cells is dependent on the microenvironment. Fibroblasts are important participants in processes such as injury, inflammation and remodeling (Fallowfield 2011). Fibroblasts are characterized by a unique ability to transdifferentiate between different types with various functionalities (Sappino et al. 1990). It has been reported previously that administration of TGF-β in rats resulted in the formation of a granulation tissue, in which, *α-SMA* expressing myofibroblasts were abundant (Desmouliere et al. 1993).

Provided that miR-15b and miR-497 have an impact on *Smad7* expression, it was hypothesized that both molecules have an impact on fibroblast differentiation. Primary lung fibroblasts were transfected with microRNA mimics or control mimics. The cells were transfected for 24 h and the expression levels of *α-SMA* was evaluated

(Fig 4-12). Transfection with miR-15b and miR-497 using normal media increased *α-SMA* expression (Fig 4-12 A). When cells were stimulated with TGF-β for 12 h, the change in expression levels of *α-SMA* between groups remained the same but the expression baseline was elevated (Fig 4-12 B). In order to evaluate whether *α-SMA* up-regulation is TGF-β dependent, prior to the application of mimic, the inhibitor SB431542 was used. This is a selective inhibitor of the TGFBRI, ALK4, ALK5 and ALK7. There was no change in *α-SMA* levels, an indication that both microRNAs act through the canonical TGF-β pathway (Fig 4-12 C).

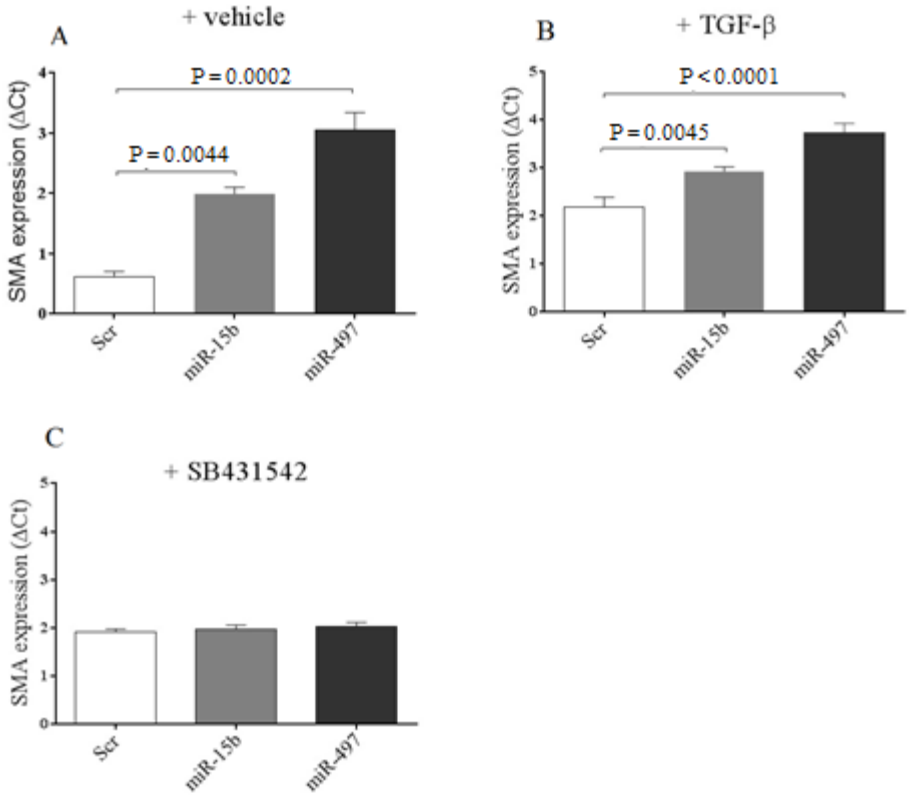

Figure 4-12 Impact of miR-15b and miR-497 on *α-SMA* in primary lung fibroblasts is TGF-β dependent.

Fibroblasts were transfected with 40 nM of control mimic (Scr), or miR-15b or miR-497 mimic for 24 h. Expression analysis of *α-SMA* gene was assessed, by real-time RT-PCR (n =4, per group). The cells were stimulated either with vehicle (A) or 5 ng/ml of TGF-β for 12 h (B), or treated with 10 nM SB431542 before transfection (C). Data are expressed as mean ± SEM. P values were determined by using 1-way ANOVA with a Bonferroni post hoc test.

In order to evaluate the impact of both microRNAs on the α-SMA protein level, primary lung fibroblasts were transfected with microRNAs and were stimulated with TGF-β. The cells were subjected to immunofluorescence analysis of α-SMA; both microRNAs caused an increased fluorescence intensity of a-SMA (Fig 4-13).

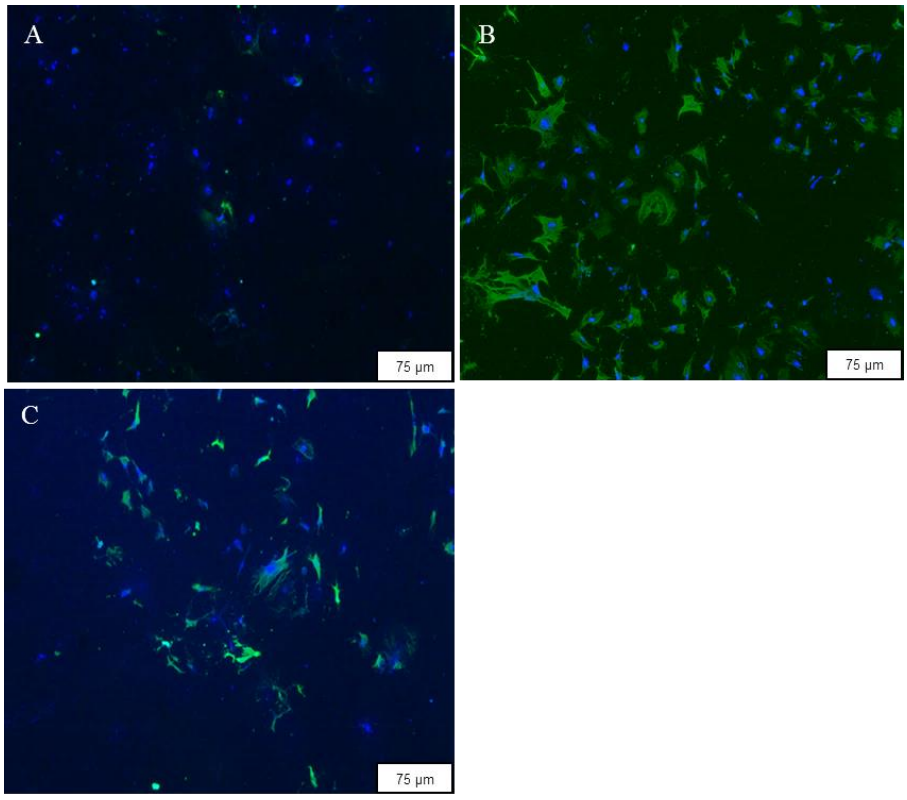

Figure 4-13 Impact of miR-15b and miR-497 on α-SMA protein levels in primary lung fibroblasts.

Fibroblasts were transfected with 40 nM control mimic (Scr) (A), or with miR-15b (B) or with miR-497 (C) for 24 h. Following transfection, 5 ng/ml of TGF-β was added to the transfection medium for additional 6 h. Immunolocalization of α-SMA (green); nuclei were stained using DAPI (blue). Images are at 10 × magnification.

4.10 *In vivo* inhibition of miR-15b and miR-497 after exposure to hyperoxia is associated with an improved lung morphology

To investigate whether modulation of microRNA expression *in vivo* has an effect on lung structure, LNA-antagomirs against miR-15b and miR-497 were administered to mouse pups after birth.

The setup of the *in vivo* experiment was as follow: Mouse pups were divided and randomized into four different groups. Two groups were exposed to hyperoxia (85% O_2) and the other two to normoxia (21% O_2). One group under normoxic and one under hyperoxic conditions were injected intraperitoneal with a control mimic microRNA (Scr) and the other two groups were injected with a mixture containing LNA-antagomir-15b and LNA-antagomir-497. The mouse pups were injected on P1 and on P3. Figure 4-14 A depicts the experimental set up. There are several studies that have reported efficient and long-lasting silencing of microRNAs using LNA-antagomirs (Stenvang et al. 2012). In the current study, two ip injections were given in two different dosages, 10 mg/kg and 20 mg/kg. The antagomirs reached the lung by P3 and efficiently down-regulated the target microRNA. As the purpose of this study was to lower slightly the expression (normalizing the increase in the expression observed after exposure to hyperoxia), the 10 mg/kg dosage was applied. The microRNA expression remained at a lower level until P14, proving the fact that antagomirs have a long lasting effect (Fig 4-14 B and C).

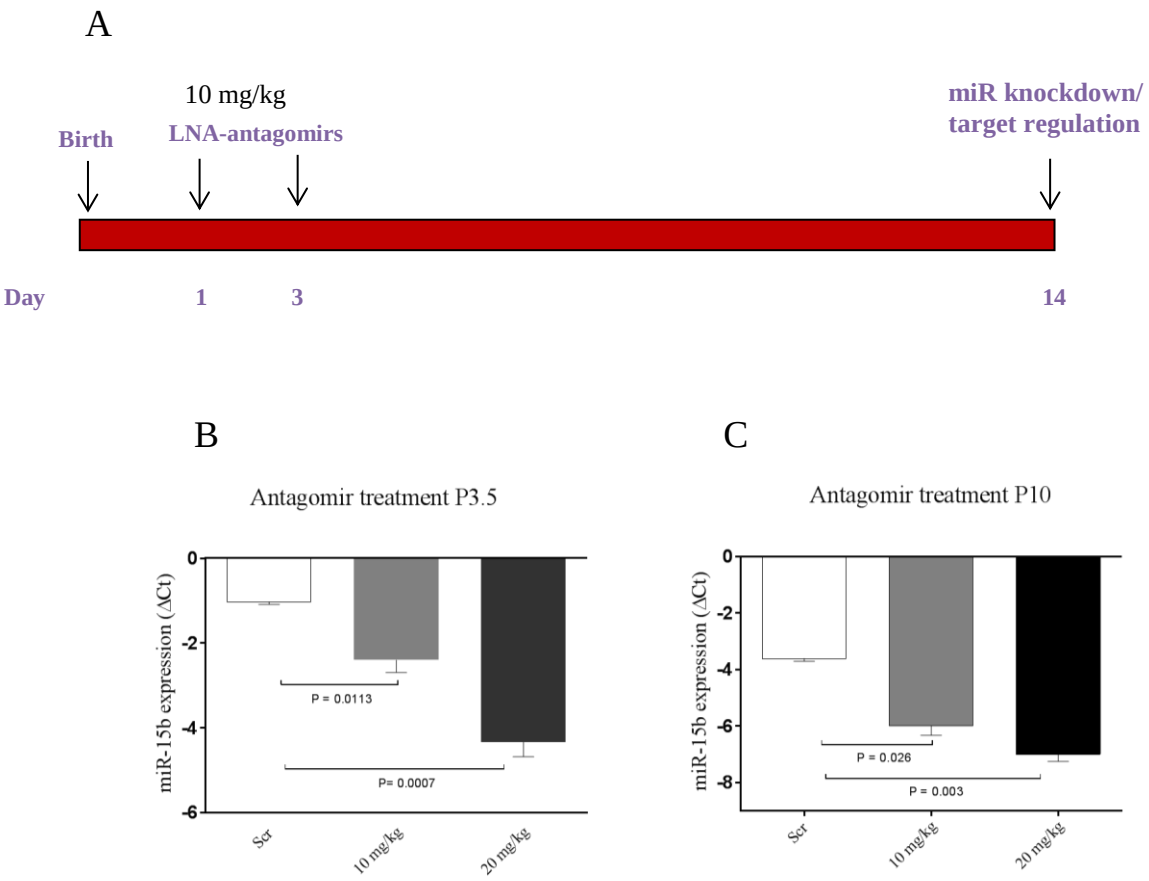

Figure 4-14 Experimental set up and an LNA-antagomir dosage response.
Pups were born and were injected intraperitoneally with 10 mg/kg on P1 and P3. Two dosages were used (10 and 20 mg/kg respectively) in order to determine the concentration for the purpose of the study. The expression level of miR-15b was analysed 48 h after the first injection (B) and on day P14 (C), prior to the extraction of the lungs. LNA, locked nucleic acid; Data are expressed as mean ± SEM. P values were determined by using 1-way ANOVA with a Bonferroni post hoc test.

The lungs were extracted on P14 and were analyzed stereologicaly using the Visiopharm software (VIS 4.5.3). Figure 4-15 depicts the lung tissue sections from mouse pups exposed to either normoxia or hyperoxia for 14 days, treated with controls or LNA-antagomirs. The lung structure was evaluated by various lung morphological parameters; there was a significant decrease in mean linear intercept (Fig 4-15 E) and a profound increase in alveoli number (Fig 4-15 F).

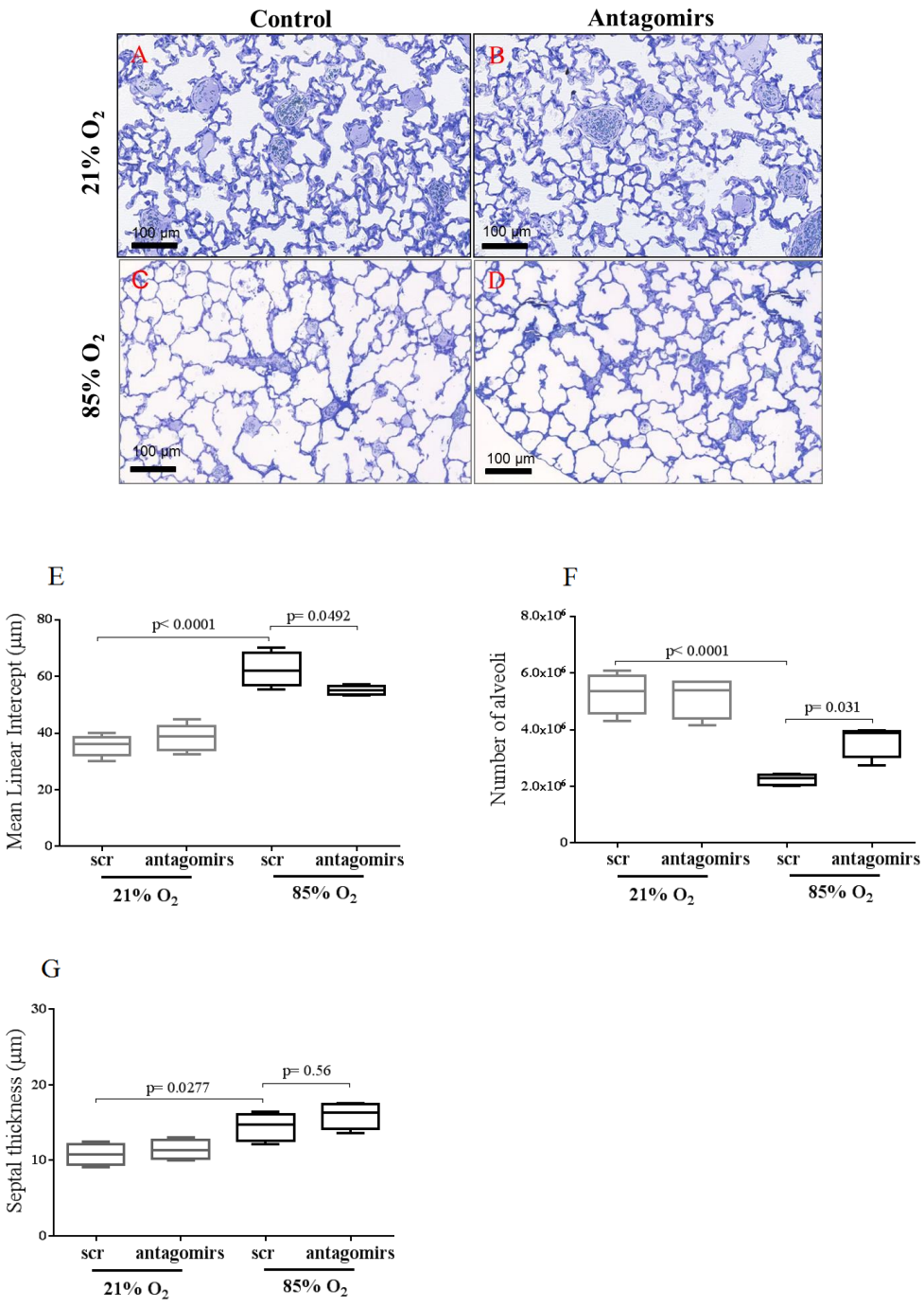

Figure 4-15 LNA-antagomir administration improved perturbed alveolar development after exposure to hyperoxia.

Mice were exposed to 21% O_2 or 85% O_2 for 14 days after birth, and received either control mimic or LNA-antagomirs mixed solution. Representative lung sections from mice at day P14, that were exposed to 21% O_2 (A and B) or 85% O_2 (C and D), with an administration of either a control mimic (A and C) or an LNA-antagomir mix (B and D). Lungs from all 4 groups were assessed for different lung structural parameters, including mean linear intercept (E), alveoli number (F) and septal wall thickness (G).

Data are presented as mean ± SEM (n=6, per group). P values were determined by using 1-way ANOVA with a Bonferonni post hoc test.

The septal thickness had no significant change but it expressed a tendency towards thickening of the septa. That possibly correlates with the fact that a down-regulation of miR-15b and miR-497 leads to an overexpression of proliferating genes as has been reported previously (Porrello et al. 2011).

4.11 *In vivo* inhibition of miR-15b and miR-497 decreases TGF-β signaling

To study the effect of the LNA-antagomirs on TGF-β signaling, groups exposed to normoxia or hyperoxia and treated either with controls or LNA-antagomirs, were investigated for the activation of TGF-β signaling pathway. The TGF-β signaling was elevated in the hyperoxia group compared to normoxia and it was decreased in the hyperoxia group treated with LNA-antagomirs (Fig 4-16).

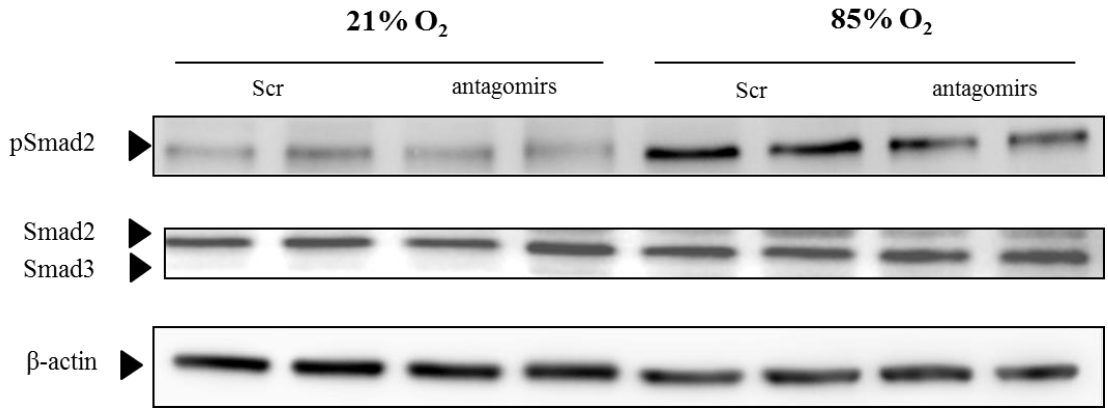

Figure 4-16 Administration of LNA-antagomirs modulates TGF-β signaling in mouse lungs.

Total cellular proteins were isolated from lungs derived from mouse pups exposed to normoxia or hyperoxia and treated either with controls or LNA-antagomirs for the first 14 days of life, subjected to immunoblot with antibodies against pSMAD2 relative to SMAD2/3 and β-ACTIN. pSmad2, phosphorylated Smad2;

To confirm that TGF-β signaling decreased after administration of the LNA-antagomirs, the expression level of a downstream ECM–related target gene of TGF-β signaling was evaluated, by real-time RT-PCR. The connective tissue growth factor

(CTGF) is a downstream gene of TGF-β signaling highly expressed in fibroblasts. *Ctgf* has been associated with TGF-β and exacerbated ECM production in conditions such as fibrosis (Brigstock 2010). *Ctgf* expression was up-regulated after exposure to hyperoxia and was normalized after administration of the LNA-antagomirs (Fig 4-17) and the finding is correlated with the data presented previously.

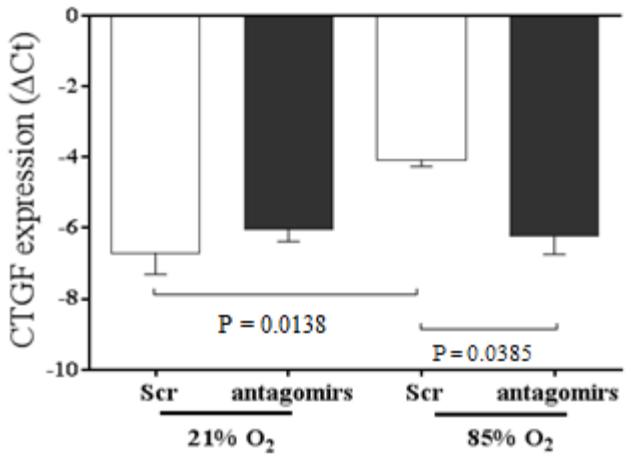

Figure 4-17 Inhibition of miR-15b and miR-497 modulates the expression of TGF-β ECM target gene.

To assess whether the LNA-antagomir administration has an effect on downstream TGF-β targets, mouse tissues were harvested for analysis on P14. The *ctgf* expression was assessed by real-time RT-PCR in the lungs of LNA-antagomir treated and control treated mice. Data are expressed as mean ± SEM. P values were determined by using 1-way ANOVA with a Bonferonni post hoc test

5 Discussion

It has been nearly 40 years since the first clinical description of BPD, but still remains one of the major complications of premature birth, bearing high costs (Short et al. 2003). Within the last decade, progress has been made but the main clinical implications persist and additional research is required to improve the outcomes of a treatment. Few of the promising scientific fields focus on stem cells and on various molecular mechanisms including epigenetic regulation. MicroRNAs are known as strong epigenetic modulators and since their discovery, research has reported that hundreds of microRNAs are implicated in various physiological processes in the body including the lung. The knowledge of microRNA involvement in the development of the lung is limited; most studies concerning the development of the lung are limited to expression level screening profiles at various stages of embryonic and late lung development (Dong et al. 2012, Lu J. et al. 2005, Williams et al. 2007). MicroRNAs such as miR-17-92 cluster (Carraro et al. 2009) can regulate gene expression responsible for epithelial differentiation and acts on branching morphogenesis during early lung development. In the current study, the dynamics and the possible roles of microRNAs during late lung development were explored. One microRNA can regulate the translation of hundreds of genes (Winter et al. 2009); however one microRNA may not be sufficient to inhibit translation, and several other microRNA species are required to bind to the mRNA repressing the expression. In the beginning of the microRNA exploration, it was thought that microRNAs bound to the RISC were able to inhibit protein synthesis by blocking protein elongation (Olsen and Ambros 1999). Most recent evidence suggested that microRNAs induce target instability. The microRNA-RISC complex initiates the degradation of mRNA by transferring it from cytosol to “P-bodies”, sites of RNA degradation (Liu J. et al. 2005). Thus, microRNAs inhibit the initiation of mRNA translation into protein.

5.1 MicroRNA-15 family expression is regulated after exposure to hyperoxia

MicroRNAs are involved in numerous biological processes but the knowledge of microRNA involvement in lung development is limited. Mice and rats with targeted de-regulation of microRNA processing develop severe developmental anomalies but the mechanisms of action in these processes are not well established (Mattes et al. 2008). The generation of transgenic animals is very promising regarding the expansion of knowledge on these mechanisms. For example the importance of miR-17-92 cluster was described in various transgenic mouse models with the knock-out resulting in postnatal lethality (Ventura et al. 2008).

In the current study, expression profiling of microRNAs during normal lung development and in lungs exposed to hyperoxia, revealed a significant number of de-regulated microRNA molecules that might play a role in modulating processes during the alveolar phase. MicroRNA-15 family expression was stably elevated during development under normoxic conditions and was highly up-regulated before the peak of secondary septation in mice. This elevated expression of microRNA-15 family may be functionally important in regulating homeostasis and various processes within the lung. In total, 67 microRNAs were deregulated during normal lung development and 55 microRNAs were deregulated after exposure to 85% O_2 for 14 days after birth. *In silico* target prediction analysis of miR-15b and miR-497 revealed 63 common gene targets with *Smad7* being one of the top candidates.

5.2 MicroRNA-15 family down-regulates Smad7 expression and enhances TGF-β canonical signaling *in vitro*

MiR-15b and miR-497, two of the most up-regulated microRNAs after exposure to hyperoxia, were chosen for this study with the hypothesis that modulate TGF-β signaling, a critical signaling network in various processes such as proliferation, apoptosis, cell cycle and overall development (Massague 2012). Several studies have reported that alterations in *Smad7* expression have been implicated in various human diseases and a potential therapeutic treatment could focus on controlling gene activity and stability (Gronroos et al. 2002, Simonsson et al. 2005). One of these studies focused on the development of antisense

inhibitors for the prevention and treatment of central nervous system such as sclerosis or immune encephalomyelitis (Kleiter et al. 2007).

Concerning fibrosis, there were two drugs that are able to restore normal levels of *Smad7* and have been proposed as therapeutic agents against interstitial fibrosis (Lu M. et al. 2009, Ning et al. 2009). One is enalapril and is an angiotensin converting enzyme and it is used in the treatment of hypertension; the second is tetramethylpyrazine and it is derived from a Chinese herb used in preventing ischemia. Both drugs were able to decrease the accumulation of lesions in the kidney through an up-regulation of Smad7 protein expression (Lu M. et al. 2009).

The conclusion of these studies supports the fact that a tuned balance between TGF-β and *Smad7* is important in maintaining homeostasis. Thus, any alteration of this balance can lead to the development of human diseases.

In the current study, *in vitro* experiments including a luciferase assay revealed the direct association of miR-15b and *Smad7* and the impact on TGF-β signaling. Overexpression of miR-15b and miR-497 in primary fibroblasts led to a decrease of *Smad7* mRNA and protein level and to an increase of TGF-β signaling. Hibio et al. have previously suggested that microRNAs with the same 'seed' sequence but different duplex structure have different efficacies and that depends on the melting temperature value of the microRNA sequence (Hibio et al. 2012). More specifically Hibio et al. have reported that the silencing efficacy of the microRNA is correlated to the melting temperature; the higher the temperature, the higher the efficacy. In the current study miR-15b and miR-497 share the same 'seed' sequence and target identical genes. However both microRNAs differ in the total sequence structure so it is assumed that the impact on genes differs. In that context, miR-497 possesses a higher melting temperature value.

Fibroblast to myofibroblast differentiation is known to be regulated by TGF-β and it is a critical procedure, dependent on the nature of cellular microenvironment, and is strongly associated with the secondary septation and the formation of definitive alveoli (Choi 2010). Alterations in the microenvironment occur during lung injury, inflammation and repair (Thannickal et al. 2003). Fibroblasts play an important role in such changes and can undergo between different cell types such as lipofibroblasts and myofibroblasts. Lipofibroblasts contain triglycerides, cholesterol esters and retinyl esters, and are localized at the base of elongating septa during alveolarization (Torday et al. 1995, Vaccaro and Brody 1978). Myofibroblasts are the source of septal elastin, are characterized by expressing markers between fibroblasts and smooth muscle cells and they possess an ability of expressing

contractile proteins such as α-SMA (Powell 2000). Persistent proliferation of myofibroblasts can lead to fibrotic diseases (Hardie et al. 2009) but also the lack of myofibroblasts lead to decreased alveolarization (Bostrom et al. 1996). Myofibroblasts are located in the developing secondary septa and the septal tips during the alveolar phase and for that reason are characterized as alveolar myofibroblasts (Dickie et al. 2008). In this study, overexpression of miR-15b and miR-497 in primary lung fibroblasts led to increased TGF-β signaling and an increase in α-SMA expression. The increase of microRNA-15 family members during hyperoxia, suggests that it is a part of a regulatory mechanism to increase TGF-β activity.

5.3 *In vivo* inhibition of miR15b and miR-497 improves lung structure and increases alveolarization

The use of antisense oligonucleotides is a promising approach that belongs to antisense therapy and there are two antisense oligonucleotides that have approved by the FDA (Perry and Balfour 1999, Santos et al. 2015). Antisense therapy can be used against various genetic diseases and it is a technique similar to RNA interference (RNAi), although the main mechanism differs. The development of antisense oligonucleotides can also be against microRNAs, with the form of locked nucleic acids (LNA), which allowed the researchers to modulate the expression of microRNAs. This interference was an indirect way to act simultaneously on the expression of hundreds of genes, suggesting greater responses in various diseases. Inhibition of microRNAs *in vivo* was first described by Hutvagner et al. (Hutvagner et al. 2004); in this study, antisense oligonucleotides complementary to let-7, were injected to *C. elegans* leading to a loss of function. The use of 3' cholesterol-conjugated, 2'-O-Me oligonucleotides called antagomirs was described in 2005 by Krutzfeldt et al. The administration of three tail vein injections of antagomir-16 resulted in inhibition of miR-16 in the kidney, liver, lung, heart, skeletal muscle, skin, fat, bone marrow and adrenal glands but not in the brain (Krutzfeldt et al. 2005). Furthermore, inhibition of miR-16 in the brain was accomplished by delivery of antagomir-16 in the mouse cortex. The recent development of LNAs was a result of multiple chemical modifications, improving nuclease resistance of the oligonucleotides and increasing the binding affinity to target microRNAs. In a study by Porello et al., microRNA-15 family was reported to regulate the expression of a number of cell cycle genes; this association suggested that inhibition of the microRNA-15

family with the use of LNA-antagomirs might increase proliferation of cardiomyocytes and decrease infarct sizes. Indeed, the LNA-antagomirs increased regeneration of the infarcted myocardium due to the proliferation of cardiomyocytes (Porrello et al. 2011).

In the current study, *in vivo* inhibition of two members of the microRNA-15 family led to three important findings. First, miR-15b and miR-497 expression was efficiently normalized during hyperoxia, by injecting 15-mer LNAs intraperitoneal in mouse pups. Second, inhibition of both microRNAs improved lung morphology by reducing mean linear intercept, increasing alveoli number by almost 50%, but had no impact on septal thickness. One major characteristic of BPD is the thickening of the septa (Bourbon et al. 2005), a characteristic that was not improved after treatment in hyperoxia group. Third, inhibition of both molecules, following LNA administration, decreased TGF-β signaling and the expression of *Ctgf*, a downstream ECM-related gene. The present study is unique in administering LNAs in a mouse model exposed to hyperoxia with an extensive lung injury and the proposed scheme is depicted in Figure 5-1. It should be noted that microRNAs have many targets and the present study does not indicate the unique contribution of *Smad7* in LNA-antagomir treated mice, resulting in the overall improvement of the lung structure. Further in vivo studies including knock out models of the specific microRNA species, the use of LNA based target site blockers are necessary to support this evidence. However, the up-regulation in the expression of microRNA-15 family target genes after antagomir administration, is correlated to proliferation, cell cycle, apoptosis and differentiation (Porrello et al. 2011) and it is likely to contribute to the lung improvement being observed.

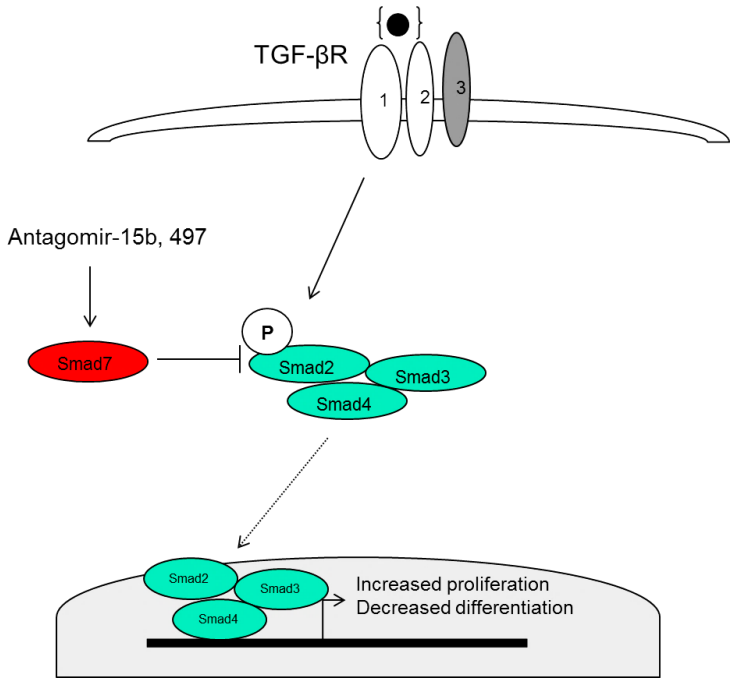

Figure 5-1 Model of TGF-β signaling regulation by using LNA-antagomirs after exposure to hyperoxia.

The antagomirs against miR-15b and miR-497 increase the expression of Smad7 and inhibit the phosphorylation of Smad2/3/4 complex. The microRNA inhibition has an impact on fibroblast differentiation and lung structure. TGF-βR, Transforming growth factor beta receptor; P, phosphorylation;

In summary, this study is the first evidence of the functionality of microRNAs in late lung development and that inhibition can improve lung morphology in mice exposed to hyperoxia from P1 to P14. Given the fact that antisense oligonucleotides entered the clinical trials, this methodology has a potential for translation (Sharma et al. 2014).

6 Summary

MicroRNAs are key regulators of organogenesis and during the last years many studies focused on microRNA expression during embryonic development. To date, there is no study to report possible roles of microRNAs in late lung development and especially during the alveolarization process.

The objective of this study was to identify microRNAs that are deregulated under hyperoxic conditions and to assess whether microRNA expression can be modulated *in vivo*. Lung microRNA expression screening was assessed at four time points under normoxic conditions by microRNA microarray; the time points were P2.5 and P3.5 (pre-septation), P5.5 (peak septation) and P14.5 (post-septation). Also, lung microRNA expression screening was assessed in pups exposed to hyperoxia (85% O_2) for 14 days. In total, 55 microRNAs were deregulated. Amongst the most up-regulated microRNAs were miR-15b and miR-497, both belong to miR-15 family. Target prediction analysis suggested that miR-15 family regulates *Smad7* expression. Using a luciferase-based reporter assay, *Smad7* was validated as a direct target of miR-15b suggesting an impact on TGF-β signaling during alveolarization. *In vitro,* overexpression of miR-15b and miR-497 down-regulated *Smad7* expression and increased TGF-β responsiveness, as assessed by a p(CAGA)$_9$ reporter assay in primary lung fibroblasts.

In vivo silencing of miR-15b and miR-497 (by using LNA-antagomirs) restored alveolarization by ~50 % in developing lungs of mouse pups exposed to hyperoxia and was assessed by using a stereological approach. The mean linear intercept (MLI) was notably decreased in the hyperoxia treated group but the septal thickness (St) remained unchanged.

These data reveal a causal role for the deregulated miR-15 family in arrested lung development associated with hyperoxia exposure. These data are also the first to report that microRNA inhibition, using LNA-antagomirs, is a viable interventional method to restore perturbed alveolarization.

7 Zusammenfassung

MicroRNAs sind die Schlüsselregulatoren der Organentwicklung. Deshalb wurde in den letzten Jahren viel auf dem Gebiet der microRNA Expression während der Embryonalentwicklung geforscht. Heutzutage gibt es noch keine Studien, welche die Rolle der microRNAs in der späten Lungenentwicklung, und besonders während der Alveolarisierung, postulieren.

Das microRNA-Screening der Lunge via microRNA microarray unter normoxischen Bedingungen ist an 4 Zeitpunkten durchgeführt worden, diese sind: P2.5 und P3.5, P5.5 und P14.5. Ebenso wurde mit Neonaten (Maus) verfahren, die für 14 Tage hyperoxischen Bedingungen ausgesetzt waren.

Insgesamt sind 55 microRNAs dereguliert. Die am meisten hochregulierten microRNAs sind miR-15b und miR-497, beide gehören zur miR-15-Familie. Anhand der target prediction Analyse wurde angedeutet, dass die miR-15-Familie die *Smad7*-Expression reguliert. Mit dem luciferase-based reporter assay wurde bestätigt, dass miR-15b ein direktes Ziel von *Smad7* ist und dies Auswirkungen auf die TGF-β Signalwirkung während der Alveolarisierung haben könnte.

In vitro hatte die Überexpression von miR-15b und miR-497 eine schwächere *Smad7*-Expression und erhöhte TGF-β Empfindlichkeit zur Folge, wie dies ebenso mit dem $p(CAGA)_9$ reporter assay in primären Lungenfibroblasten bestätigt wurde.

In vivo Silencing von miR-15b und miR-497 (mit LNA-antagomirs) führt zu einer Wiederherstellung der Alveolarisierung von ~50 % in Neonaten (Maus), die hyperoxischen Bedingungen ausgesetzt waren. Die Auswertung erfolgte hierbei mit einem Stereologieverfahren. Der mean linear intersept (MLI) ist in der hyperoxischen Gruppe erheblich reduziert wobei die Septumdicke unverändert bleibt.

Diese Ergebnisse zeigen einen kausalen Zusammenhang zwischen deregulierten microRNAs der miR-15-Familie und gehemmter Lungenentwicklung unter hyperoxischen Bedingungen. Weiterhin zeigen diese Ergebnisse, dass Inhibierung der microRNA mit LNA-antagomirs eine praktikable Therapie für gestörte Alveolarisierungsprozesse sein kann.

8 Literature

Alejandre-Alcazar MA, et al. 2008. TGF-beta signaling is dynamically regulated during the alveolarization of rodent and human lungs. Dev Dyn 237: 259-269.

Alejandre-Alcazar MA, et al. 2007. Hyperoxia modulates TGF-beta/BMP signaling in a mouse model of bronchopulmonary dysplasia. Am J Physiol Lung Cell Mol Physiol 292: 27.

Bancalari E, Claure N. 2006. Definitions and diagnostic criteria for bronchopulmonary dysplasia. Semin Perinatol 30: 164-170.

Bhaskaran M, Wang Y, Zhang H, Weng T, Baviskar P, Guo Y, Gou D, Liu L. 2009. MicroRNA-127 modulates fetal lung development. Physiol Genomics 37: 268-278.

Bhatt AJ, Pryhuber GS, Huyck H, Watkins RH, Metlay LA, Maniscalco WM. 2001. Disrupted pulmonary vasculature and decreased vascular endothelial growth factor, Flt-1, and TIE-2 in human infants dying with bronchopulmonary dysplasia. Am J Respir Crit Care Med 164: 1971-1980.

Boros LG, Torday JS, Paul Lee W-N, Rehan VK. 2002. Oxygen-induced metabolic changes and transdifferentiation in immature fetal rat lung lipofibroblasts. Molecular Genetics and Metabolism 77: 230-236.

Bostrom H, et al. 1996. PDGF-A signaling is a critical event in lung alveolar myofibroblast development and alveogenesis. Cell 85: 863-873.

Boucher E, Provost PR, Plante J, Tremblay Y. 2009. Androgen receptor and 17beta-HSD type 2 regulation in neonatal mouse lung development. Mol Cell Endocrinol 311: 109-119.

Bourbon J, Boucherat O, Chailley-Heu B, Delacourt C. 2005. Control Mechanisms of Lung Alveolar Development and Their Disorders in Bronchopulmonary Dysplasia. Pediatr Res 57: 38R-46R.

Bozyk PD, Bentley JK, Popova AP, Anyanwu AC, Linn MD, Goldsmith AM, Pryhuber GS, Moore BB, Hershenson MB. 2012. Neonatal periostin knockout mice are protected from hyperoxia-induced alveolar simplication. PLoS ONE 7: 17.

Brigstock DR. 2010. Connective tissue growth factor (CCN2, CTGF) and organ fibrosis: lessons from transgenic animals. J Cell Comm and Signal 4: 1-4.

Briones-Orta MA, Tecalco-Cruz AC, Sosa-Garrocho M, Caligaris C, Macias-Silva M. 2011. Inhibitory Smad7: emerging roles in health and disease. Curr Mol Pharmacol 4: 141-153.

Buckley S, Warburton D. 2002. Dynamics of metalloproteinase-2 and -9, TGF-beta, and uPA activities during normoxic vs. hyperoxic alveolarization. Am J Physiol Lung Cell Mol Physiol 283: L747-754.

Cai X, Hagedorn CH, Cullen BR. 2004. Human microRNAs are processed from capped, polyadenylated transcripts that can also function as mRNAs. Rna 10: 1957-1966.

Carraro G, et al. 2009. miR-17 family of microRNAs controls FGF10-mediated embryonic lung epithelial branching morphogenesis through MAPK14 and STAT3 regulation of E-Cadherin distribution. Dev Biol 333: 238-250.

Chamorro-Jorganes A, Araldi E, Penalva LOF, Sandhu D, Fernández-Hernando C, Suárez Y. 2011. MicroRNA-16 and MicroRNA-424 regulate cell-autonomous angiogenic functions in endothelial cells via targeting VEGFR2 and FGFR1. Arterioscler. Thromb. Vasc. Biol. 31: 2595-2606.

Choi CW. 2010. Lung interstitial cells during alveolarization. Korean Journal of Pediatrics 53: 979-984.

Coalson JJ. 2006. Pathology of bronchopulmonary dysplasia. Semin Perinatol 30: 179-184.

Crapo JD, Barry BE, Gehr P, Bachofen M, Weibel ER. 1982. Cell number and cell characteristics of the normal human lung. Am Rev Respir Dis 126: 332-337.

Davis BN, Hilyard AC, Lagna G, Hata A. 2008. SMAD proteins control DROSHA-mediated microRNA maturation. Nature 454: 56-61.

Desmouliere A, Geinoz A, Gabbiani F, Gabbiani G. 1993. Transforming growth factor-beta 1 induces alpha-smooth muscle actin expression in granulation tissue myofibroblasts and in quiescent and growing cultured fibroblasts. J Cell Biol 122: 103-111.

Dickie R, Wang YT, Butler JP, Schulz H, Tsuda A. 2008. Distribution and quantity of contractile tissue in postnatal development of rat alveolar interstitium. Anat Rec 291: 83-93.

Dong J, Jiang G, Asmann YW, Tomaszek S, Jen J, Kislinger T, Wigle DA. 2010. MicroRNA networks in mouse lung organogenesis. PLoS ONE 5: 0010854.

Dong J, et al. 2012. MicroRNA-mRNA interactions in a murine model of hyperoxia-induced bronchopulmonary dysplasia. BMC Genom 13: 1471-2164.

Fallowfield JA. 2011. Therapeutic targets in liver fibrosis. Am J Physiol Gastrointest Liver Physiol 300: 13.

Fineberg SK, Kosik KS, Davidson BL. 2009. MicroRNAs potentiate neural development. Neuron 64: 303-309.

Friedman RC, Farh KK, Burge CB, Bartel DP. 2009. Most mammalian mRNAs are conserved targets of microRNAs. Genome Res 19: 92-105.

Gangaraju VK, Lin H. 2009. MicroRNAs: key regulators of stem cells. Nat Rev Mol Cell Biol 10: 116-125.

Gauldie J, Galt T, Bonniaud P, Robbins C, Kelly M, Warburton D. 2003. Transfer of the Active Form of Transforming Growth Factor-β1 Gene to Newborn Rat Lung Induces Changes Consistent with Bronchopulmonary Dysplasia. Am J Pathol 163: 2575-2584.

Goldin GV, Wessells NK. 1979. Mammalian lung development: the possible role of cell proliferation in the formation of supernumerary tracheal buds and in branching morphogenesis. J Exp Zool 208: 337-346.

Grishok A, Pasquinelli AE, Conte D, Li N, Parrish S, Ha I, Baillie DL, Fire A, Ruvkun G, Mello CC. 2001. Genes and mechanisms related to RNA interference regulate expression of the small temporal RNAs that control C. elegans developmental timing. Cell 106: 23-34.

Gronroos E, Hellman U, Heldin CH, Ericsson J. 2002. Control of Smad7 stability by competition between acetylation and ubiquitination. Mol Cell 10: 483-493.

Hardie WD, Glasser SW, Hagood JS. 2009. Emerging concepts in the pathogenesis of lung fibrosis. Am J Pathol 175: 3-16.

Harris KS, Zhang Z, McManus MT, Harfe BD, Sun X. 2006. Dicer function is essential for lung epithelium morphogenesis. Proc Natl Acad Sci USA 103: 2208-2213.

He L, et al. 2007. A microRNA component of the p53 tumour suppressor network. Nature 447: 1130-1134.

Hibio N, Hino K, Shimizu E, Nagata Y, Ui-Tei K. 2012. Stability of miRNA 5'terminal and seed regions is correlated with experimentally observed miRNA-mediated silencing efficacy. Sci Rep 2: 18.

Hislop AA. 2002. Airway and blood vessel interaction during lung development. J Anat 201: 325-334.

Hsia CC, Hyde DM, Ochs M, Weibel ER. 2010. An official research policy statement of the American Thoracic Society/European Respiratory Society: standards for quantitative assessment of lung structure. Am J Respir Crit Care Med 181: 394-418.

Hutvagner G, Simard MJ, Mello CC, Zamore PD. 2004. Sequence-specific inhibition of small RNA function. PLoS Biol 2: 24.

Hutvagner G, McLachlan J, Pasquinelli AE, Balint E, Tuschl T, Zamore PD. 2001. A cellular function for the RNA-interference enzyme Dicer in the maturation of the let-7 small temporal RNA. Science 293: 834-838.

Imamura T, Takase M, Nishihara A, Oeda E, Hanai J, Kawabata M, Miyazono K. 1997. Smad6 inhibits signalling by the TGF-beta superfamily. Nature 389: 622-626.

Iwasaki S, Kawamata T, Tomari Y. 2009. Drosophila argonaute1 and argonaute2 employ distinct mechanisms for translational repression. Mol Cell 34: 58-67.

Jobe AH. 2011. The New Bronchopulmonary Dysplasia. Current Opinion in Pediatrics 23: 167-172.

Kasai H, Allen JT, Mason RM, Kamimura T, Zhang Z. 2005. TGF-beta1 induces human alveolar epithelial to mesenchymal cell transition (EMT). Respir Res 6: 56.

Kitaoka H, Burri PH, Weibel ER. 1996. Development of the human fetal airway tree: analysis of the numerical density of airway endtips. Anat Rec 244: 207-213.

Kleiter I, Pedré X, Mueller AM, Poeschl P, Couillard-Despres S, Spruss T, Bogdahn U, Giegerich G, Steinbrecher A. 2007. Inhibition of Smad7, a negative regulator of TGF-beta signaling, suppresses autoimmune encephalomyelitis. J Neuroim 187: 61-73.

Knudsen L, Weibel ER, Gundersen HJG, Weinstein FV, Ochs M. 2010. Assessment of air space size characteristics by intercept (chord) measurement: an accurate and efficient stereological approach. J Appl Physiol 108: 412-421.

Koshida S, Hirai Y. 1997. Identification of cellular recognition sequence of epimorphin and critical role of cell/epimorphin interaction in lung branching morphogenesis. Biochem Biophys Res Commun 234: 522-525.

Kotecha S, Kotecha SJ. 2012. Long term respiratory outcomes of perinatal lung disease: Semin Fetal Neonatal Med. 2012 Apr;17(2):65-6. doi: 10.1016/j.siny.2012.01.001. Epub 2012 Jan 23.

Kotecha S, Wangoo A, Silverman M, Shaw RJ. 1995. Increase in the concentration of transforming growth factor beta-1 in bronchoalveolar lavage fluid before development of chronic lung disease of prematurity. J Pediatr 128: 464-469.

Krutzfeldt J, Rajewsky N, Braich R, Rajeev KG, Tuschl T, Manoharan M, Stoffel M. 2005. Silencing of microRNAs in vivo with 'antagomirs'. Nature 438: 685-689.

Kumarasamy A, et al. 2009. Lysyl oxidase activity is dysregulated during impaired alveolarization of mouse and human lungs. Am J Respir Crit Care Med 180: 1239-1252.

Lecart C, Cayabyab R, Buckley S, Morrison J, Kwong KY, Warburton D, Ramanathan R, Jones CA, Minoo P. 2000. Bioactive transforming growth factor-beta in the lungs of extremely low birthweight neonates predicts the need for home oxygen supplementation. Biol Neonate 77: 217-223.

Lemons JA, et al. 2001. Very low birth weight outcomes of the National Institute of Child health and human development neonatal research network, January 1995 through December 1996. NICHD Neonatal Research Network. Pediatrics 107.

Lewis BP, Burge CB, Bartel DP. Conserved seed pairing, often flanked by adenosines, indicates that thousands of human genes are microRNA targets: Cell. 2005 Jan 14;120(1):15-20.

Liu G, Friggeri A, Yang Y, Milosevic J, Ding Q, Thannickal VJ, Kaminski N, Abraham E. 2010. miR-21 mediates fibrogenic activation of pulmonary fibroblasts and lung fibrosis. J Exp Med 207: 1589-1597.

Liu J, Rivas FV, Wohlschlegel J, Yates JR, 3rd, Parker R, Hannon GJ. 2005. A role for the P-body component GW182 in microRNA function. Nat Cell Biol 7: 1261-1266.

Liu Y, Martinez L, Ebine K, Abe MK. 2008. Role for mitogen-activated protein kinase p38α in lung epithelial branching morphogenesis. Developm Biol 314: 224-235.

Lu J, Qian J, Chen F, Tang X, Li C, Cardoso WV. 2005. Differential expression of components of the microRNA machinery during mouse organogenesis. Biochem Biophys Res Commun 334: 319-323.

Lu M, Zhou J, Wang F, Liu Y, Zhang Y. 2009. [Effect of tetramethylpyrazine on expression of Smad7 and SnoN in rats with UUO]. Zhongguo Zhong Yao Za Zhi 34: 84-88.

Lujambio A, et al. 2008. A microRNA DNA methylation signature for human cancer metastasis. Proc Natl Acad Sci U S A 105: 13556-13561.

Lund E, Guttinger S, Calado A, Dahlberg JE, Kutay U. 2004. Nuclear export of microRNA precursors. Science 303: 95-98.

Makinde T, Murphy RF, Agrawal DK. 2007. The regulatory role of TGF-beta in airway remodeling in asthma. Immunol Cell Biol 85: 348-356.

Massague J. 2012. TGF[beta] signalling in context. Nat Rev Mol Cell Biol 13: 616-630.

Mattes J, Collison A, Foster PS. 2008. Emerging role of microRNAs in disease pathogenesis and strategies for therapeutic modulation. Curr Opin Mol Ther 10: 150-157.

Miyazono K, Maeda S, Imamura T. 2005. BMP receptor signaling: transcriptional targets, regulation of signals, and signaling cross-talk. Cytokine Growth Factor Rev 16: 251-263.

Mund SI, Stampanoni M, Schittny JC. 2008. Developmental alveolarization of the mouse lung. Dev Dyn 237: 2108-2116.

Nabeyrat E, Corroyer S, Besnard V, Cazals-Laville V, Bourbon J, Clement A. 2001. Retinoic acid protects against hyperoxia-mediated cell-cycle arrest of lung alveolar epithelial cells by preserving late G1 cyclin activities. Am J Respir Cell Mol Biol 25: 507-514.

Nakanishi H, Sugiura T, Streisand JB, Lonning SM, Roberts JD, Jr. 2007. TGF-beta-neutralizing antibodies improve pulmonary alveologenesis and vasculogenesis in the injured newborn lung. Am J Physiol Lung Cell Mol Physiol 293: 30.

Nakao A, et al. 1997. Identification of Smad7, a TGFbeta-inducible antagonist of TGF-beta signalling. Nature 389: 631-635.

Neptune ER, Frischmeyer PA, Arking DE, Myers L, Bunton TE, Gayraud B, Ramirez F, Sakai LY, Dietz HC. 2003. Dysregulation of TGF-[beta] activation contributes to pathogenesis in Marfan syndrome. Nat Genet 33: 407-411.

Nicolas FE. 2011. Experimental validation of microRNA targets using a luciferase reporter system. Methods Mol Biol 732: 139-152.

Ning W, Tao L, Liu C, Sun J, Xiao Y, Hu J, Chen J, Zheng X, Wang W. 2009. [Effect of enalapril on the expression of TGF-beta1, p-Smad2/3 and Smad7 in renal interstitial fibrosis in rats]. Zhong Nan Da Xue Xue Bao Yi Xue Ban 34: 27-34.

Northway WH, Jr., Rosan RC, Porter DY. 1967. Pulmonary disease following respirator therapy of hyaline-membrane disease. Bronchopulmonary dysplasia. N Engl J Med 276: 357-368.

O'Donnell KA, Wentzel EA, Zeller KI, Dang CV, Mendell JT. 2005. c-Myc-regulated microRNAs modulate E2F1 expression. Nature 435: 839-843.

Olsen PH, Ambros V. 1999. The lin-4 regulatory RNA controls developmental timing in Caenorhabditis elegans by blocking LIN-14 protein synthesis after the initiation of translation. Dev Biol 216: 671-680.

Perry CM, Balfour JA. 1999. Fomivirsen. Drugs 57: 375-380.

Porrello ER, Johnson BA, Aurora AB, Simpson E, Nam YJ, Matkovich SJ, Dorn GW, 2nd, van Rooij E, Olson EN. 2011. MiR-15 family regulates postnatal mitotic arrest of cardiomyocytes. Circ Res 109: 670-679.

Powell DW. 2000. Myofibroblasts: paracrine cells important in health and disease. Transactions of the American Clinical and Climatological Association 111: 271-293.

Saito Y, Liang G, Egger G, Friedman JM, Chuang JC, Coetzee GA, Jones PA. 2006. Specific activation of microRNA-127 with downregulation of the proto-oncogene BCL6 by chromatin-modifying drugs in human cancer cells. Cancer Cell 9: 435-443.

Santos RD, Raal FJ, Catapano AL, Witztum JL, Steinhagen-Thiessen E, Tsimikas S. 2015. Mipomersen, an Antisense Oligonucleotide to Apolipoprotein B-100, Reduces Lipoprotein(a) in Various Populations With Hypercholesterolemia: Results of 4 Phase III Trials. Arterioscler Thromb Vasc Biol 35: 689-699.

Sappino AP, Schurch W, Gabbiani G. 1990. Differentiation repertoire of fibroblastic cells: expression of cytoskeletal proteins as marker of phenotypic modulations. Lab Invest 63: 144-161.

Schittny JC, Mund SI, Stampanoni M. 2008. Evidence and Structural Mechanism for Late Lung Alveolarization. Proc A T S 5: 360-360.

Schmid P, Cox D, Bilbe G, Maier R, McMaster GK. 1991. Differential expression of TGF beta 1, beta 2 and beta 3 genes during mouse embryogenesis. Development 111: 117-130.

Schreiber MD, Gin-Mestan K, Marks JD, Huo D, Lee G, Srisuparp P. 2003. Inhaled nitric oxide in premature infants with the respiratory distress syndrome. N Engl J Med 349: 2099-2107.

Seluanov A, Vaidya A, Gorbunova V. 2010. Establishing Primary Adult Fibroblast Cultures From Rodents. Journal of Visualized Experiments : JoVE: 2033.

Sharma VK, Sharma RK, Singh SK. 2014. Antisense oligonucleotides: modifications and clinical trials. MedChemComm 5: 1454-1471.

Short EJ, Klein NK, Lewis BA, Fulton S, Eisengart S, Kercsmar C, Baley J, Singer LT. 2003. Cognitive and academic consequences of bronchopulmonary dysplasia and very low birth weight: 8-year-old outcomes. Pediatrics 112.

Simonsson M, Heldin CH, Ericsson J, Gronroos E. 2005. The balance between acetylation and deacetylation controls Smad7 stability. J Biol Chem 280: 21797-21803.

Sokol JP, Schiemann WP. 2004. Cystatin C antagonizes transforming growth factor beta signaling in normal and cancer cells. Mol Cancer Res 2: 183-195.

Sokol JP, Neil JR, Schiemann BJ, Schiemann WP. 2005. The use of cystatin C to inhibit epithelial-mesenchymal transition and morphological transformation stimulated by transforming growth factor-beta. Breast Cancer Res 7: 23.

Song G, Wang L. 2008. Transcriptional mechanism for the paired miR-433 and miR-127 genes by nuclear receptors SHP and ERRγ. Nucleic Acids Research 36: 5727-5735.

Sood P, Krek A, Zavolan M, Macino G, Rajewsky N. 2006. Cell-type-specific signatures of microRNAs on target mRNA expression. Proc Natl Acad Sci U S A 103: 2746-2751.

Stenvang J, Petri A, Lindow M, Obad S, Kauppinen S. 2012. Inhibition of microRNA function by antimiR oligonucleotides. Silence 3: 3-1.

Thannickal VJ, Lee DY, White ES, Cui Z, Larios JM, Chacon R, Horowitz JC, Day RM, Thomas PE. 2003. Myofibroblast differentiation by transforming growth factor-beta1 is dependent on cell adhesion and integrin signaling via focal adhesion kinase. J Biol Chem 278: 12384-12389.

Torday J, Hua J, Slavin R. 1995. Metabolism and fate of neutral lipids of fetal lung fibroblast origin. Biochim Biophys Acta 20: 198-206.

Tschanz SA, Burri PH, Weibel ER. 2011. A simple tool for stereological assessment of digital images: the STEPanizer. J Microsc 243: 47-59.

Vaccaro C, Brody JS. 1978. Ultrastructure of developing alveoli. I. The role of the interstitial fibroblast. Anat Rec 192: 467-479.

Valencia-Sanchez MA, Liu J, Hannon GJ, Parker R. 2006. Control of translation and mRNA degradation by miRNAs and siRNAs. Genes Dev 20: 515-524.

Ventura A, et al. 2008. Targeted deletion reveals essential and overlapping functions of the miR-17 through 92 family of miRNA clusters. Cell 132: 875-886.

Vicencio AG, Lee CG, Cho SJ, Eickelberg O, Chuu Y, Haddad GG, Elias JA. 2004. Conditional overexpression of bioactive transforming growth factor-beta1 in neonatal mouse lung: a new model for bronchopulmonary dysplasia? Am J Respir Cell Mol Biol 31: 650-656.

Walsh MC, et al. 2004. Impact of a physiologic definition on bronchopulmonary dysplasia rates. Pediatrics 114: 1305-1311.

Watanabe Y, Tomita M, Kanai A. 2007. Computational methods for microRNA target prediction. Methods Enzymol 427: 65-86.

Weibel ER. 1963. Principles and methods for the morphometric study of the lung and other organs. Lab Invest 12: 131-155.

Williams AE, Moschos SA, Perry MM, Barnes PJ, Lindsay MA. 2007. Maternally imprinted microRNAs are differentially expressed during mouse and human lung development. Dev Dyn 236: 572-580.

Winter J, Jung S, Keller S, Gregory RI, Diederichs S. 2009. Many roads to maturity: microRNA biogenesis pathways and their regulation. Nat Cell Biol 11: 228-234.

Wu S, Peng J, Duncan MR, Kasisomayajula K, Grotendorst G, Bancalari E. 2007. ALK-5 Mediates Endogenous and TGF-β1–Induced Expression of Connective Tissue Growth Factor in Embryonic Lung. Ame J Respir Cell Mol Biol 36: 552-561.

Yi R, Qin Y, Macara IG, Cullen BR. 2003. Exportin-5 mediates the nuclear export of pre-microRNAs and short hairpin RNAs. Genes Dev 17: 3011-3016.

Yue J, Tigyi G. 2010. Conservation of miR-15a/16-1 and miR-15b/16-2 clusters. Mamm Genome 21: 88-94.

Zeng X, Gray M, Stahlman MT, Whitsett JA. 2001. TGF-beta1 perturbs vascular development and inhibits epithelial differentiation in fetal lung in vivo. Dev Dyn 221: 289-301.

Zhao J, Lee M, Smith S, Warburton D. 1998. Abrogation of Smad3 and Smad2 or of Smad4 gene expression positively regulates murine embryonic lung branching morphogenesis in culture. Dev Biol 194: 182-195.

Zhou L, Dey CR, Wert SE, Whitsett JA. 1996. Arrested lung morphogenesis in transgenic mice bearing an SP-C-TGF-beta 1 chimeric gene. Dev Biol 175: 227-238.

Zhu L, Chen S, Chen Y. 2011. Unraveling the biological functions of Smad7 with mouse models. Cell Biosci 1: 2045-3701.

9 Acknowledgements

I would like to express my gratitude to my supervisor Dr. Rory E. Morty for his assistance on this project. He accepted me in the MBML graduate program and he taught me to think critically, to evaluate scientific literature and be attentive to details when we conduct research.

I would like to thank Prof. Werner Seeger for his inspirational talks and the joyful criticism in every journal club and scientific meeting. He has been understanding and he appreciated the student's efforts.

I would like to thank all the Morty lab members for the funny and the serious moments in every day lab life. Especially Gero Niess, Simone Becker, Lukasz Wujak, for the experimental and even the personal advice and support. They were great in every moment and directed me with great enthusiasm. Their friendship is priceless.

My friend and colleague Tania Likhoshvay that had thousands coffees with me, during our PhD life; we supported each other in order to get through the difficult moments and we cooperated in many projects and produced a lot of work. I am really grateful.

A big hearted thank you to Julia B. for her support in everyday life. In the moments that everything looked meaningless, she was there and reminded me that life is a road with ups and downs. That is how it is supposed to be.

A big thank you to my friend Joe; he supported me in my decision to leave everything behind and join the PhD path and it is something that I will never forget.

Last but not least; my parents and my brother for their support in every little or big step that I made in this life. Without them, I would not stand here, at this moment.

10 Declaration

Hiermit erkläre ich, dass ich die vorliegende Arbeit selbständig und ohne unzulässige Hilfe oder Benutzung anderer als der angegebenen Hilfsmittel angefertigt habe. Alle Textstellen, die wörtlich oder sinngemäß aus veröffentlichten oder nichtveröffentlichten Schriften entnommen sind, und alle Angaben, die auf mündlichen Auskünften beruhen, sind als solche kenntlich gemacht. Bei den von mir durchgeführten und in der Dissertation erwähnten Untersuchungen habe ich die Grundsätze guter wissenschaftlicher Praxis, wie sie in der „Satzung der Justus-Liebig-Universität Gießen zur Sicherung guter wissenschaftlicher Praxis“ niedergelegt sind, eingehalten sowie ethische, datenschutzrechtliche und tierschutzrechtliche Grundsätze befolgt. Ich versichere, dass Dritte von mir weder unmittelbar noch mittelbar geldwerte Leistungen für Arbeiten erhalten haben, die im Zusammenhang mit dem Inhalt der vorgelegten Dissertation stehen, oder habe diese nachstehend spezifiziert. Die vorgelegte Arbeit wurde weder im Inland noch im Ausland in gleicher oder ähnlicher Form einer anderen Prüfungsbehörde zum Zweck einer Promotion oder eines anderen Prüfungsverfahrens vorgelegt. Alles aus anderen Quellen und von anderen Personen übernommene Material, das in der Arbeit verwendet wurde oder auf das direkt Bezug genommen wird, wurde als solches kenntlich gemacht. Insbesondere wurden alle Personen genannt, die direkt und indirekt an der Entstehung der vorliegenden Arbeit beteiligt waren. Mit der Überprüfung meiner Arbeit durch eine Plagiatserkennungssoftware bzw. ein internetbasiertes Softwareprogramm erkläre ich mich einverstanden.

_____ _____

Ort, Datum Unterschrift